Bull Earthquake Eng (2010) 8:535–570
DOI 10.1007/s10518-009-9159-9

ORIGINAL RESEARCH PAPER

On the repeatability and consistency of three-component ambient vibration array measurements

Brigitte Endrun · Matthias Ohrnberger · Alexandros Savvaidis

Received: 29 May 2009 / Accepted: 8 September 2009 / Published online: 3 October 2009

Abstract Ambient vibration measurements with small, temporary arrays that produce estimates of surface wave dispersion have become increasingly popular as a low-cost, non-invasive tool for site characterisation. An important requirement for these measurements to be meaningful, however, is the temporal consistency and repeatability of the resulting dispersion and spatial autocorrelation curve estimates. Data acquired within several European research projects (NERIES task JRA4, SESAME, and other multinational experiments) offer the chance to investigate the variability of the derived data products. The dataset analysed here consists of repeated array measurements, with several years of time elapsed between them. The measurements were conducted by different groups in different seasons, using different instrumentations and array layouts, at six sites in Greece and Italy. Ambient vibration amplitude spectra and locations of dominant sources vary between the two measurements at each location. Still, analysis indicates that this does not influence the derived dispersion information, which is stable in time and neither influenced by the instrumentation nor the analyst. The frequency range over which the dispersion curves and spatial autocorrelation curves can be reliably estimated depends on the array dimensions (minimum and maximum aperture) used in the specific deployment, though, and may accordingly vary between the repeated experiments. The relative contribution of Rayleigh and Love waves to the wavefield can likewise change between repeated measurements. The observed relative contribution of Rayleigh waves is generally at or below 50%, with especially low values for the rural sites. Besides, the visibility of higher modes depends on the noise wavefield conditions. The similarity of the dispersion and autocorrelation curves measured at each site indicates

B. Endrun (✉) · M. Ohrnberger
Institute of Geosciences, Potsdam University, Karl-Liebknecht-Str. 24, 14476 Potsdam, Germany
e-mail: brigitte.endrun@rub.de

M. Ohrnberger
e-mail: mao@geo.uni-potsdam.de

A. Savvaidis
Institute of Earthquake Seismology and Earthquake Engineering, G Scholis 46, Finikas,
57001 Thessaloniki, Greece
e-mail: alekos@itsak.gr

that the curves are stable, mainly determined by the sub-surface structure, and can thus be used to derive velocity information with depth. Differences between velocity models for the same site derived from independently determined dispersion and autocorrelation curves—as observed in other studies—are consequently not adequately explained by uncertainties in the measurement part.

Keywords Ambient vibrations · Surface waves · Dispersion curves · Spatial autocorrelation curves · Noise wavefield · Site characterisation

1 Introduction

Ambient vibration measurements with small, temporary arrays that produce estimates of Rayleigh and Love wave dispersion have become increasingly popular for site characterisation, with publications about improvements of measurement and processing techniques steadily growing in number (e.g. Ohori et al. 2002; Cho et al. 2004, 2006a,b; Chávez-García et al. 2005; Roberts and Asten 2005, 2007; Wathelet et al. 2005, 2008; Tada et al. 2006; Köhler et al. 2007; Fäh et al. 2008; García-Jerez et al. 2008; Gouédard et al. 2008; Morikawa and Udagawa 2009). The appeal of these methods is due to several properties: their non-destructiveness, for example in comparison to borehole measurements; their ease of use and cost-effectiveness (e.g. in comparison to active seismics with large sources like vibrators or explosives, and to the drilling of boreholes); their relatively fast operability (one day of measurements at a given site); and their larger penetration depth (up to several 100 m) compared to active seismics with a hammer source. All of these characteristics make them well-suited for measurements in densely populated areas. An important requirement for these measurements to be meaningful in the study of site effects, though, is the temporal consistency and repeatability of the resulting dispersion estimates. A recent blind test on ambient vibration data which involved field measurements, determination of dispersion and autocorrelation curves, and the inversion of these curves to determine S-velocity depth profiles showed considerable variability between results, at shallow depth as well as down to several 100 m (Cornou et al. 2009). From these results alone, however, it is impossible to decide whether the observed variability is due to differences in the measurement or in the inversion stage. Possible influences on the measurements include seasonal and more short-term (within hours or days) variations in the location, type and strength of noise sources, as well as temporal variability of the shallow ground structure, caused for example by seasonal variations in hydrological parameters (ground water level).

It is well known that instantaneous changes in shallow crustal elastic parameters can result from catastrophic events, e.g. heavy rainfall (Rigo et al. 2008), fracturing by large earthquakes (e.g. Peng and Ben-Zion 2006), stress build-up in volcanoes prior to an eruption (Wegler et al. 2006) or stress drop after an earthquake (Nishimura et al. 2000). Theoretical calculations have shown that more gradual seasonal rainfall variations, via influencing ground water level and thus shallow crustal velocities, may also result in up to 10% amplitude variations for the H/V peak at long periods (Tanimoto et al. 2006). Sens-Schönfelder and Wegler (2006) and Wang et al. (2008) observe velocity perturbations in the shallow subsurface down to several tens of metres depth due to precipitation. In a tropical environment, the velocity changes can amount to more than 10% (Sens-Schönfelder and Wegler 2006). Wang et al. (2008) also report diurnal cyclic velocity variations of significantly smaller amplitudes around 1% that they interpret as response to barometric pressure. Mucciarelli et al. (2003) find a weak negative correlation between H/V peak frequency variations and the amount of rainfall preceding

the measurements. They attribute these observations to the strong influence of various degrees of soil saturation on P-wave velocities and vertical component amplification (Yang and Sato 2000). From active seismics, Beilecke et al. (2008) describe phase shifts of 180° between surface waves generated by a high-frequency vibrator source at different times of the same day. They tentatively ascribe these variations to varying near-surface moisture content.

The variability of sources is another important issue in noise analysis. At long periods ($\geq$ 5 s), very strong inter-annual variations in the spectral amplitudes of noise are observed at seismological broad-band stations (e.g. McNamara and Buland 2004; Tanimoto et al. 2006; Aster et al. 2008). Amplitudes are largest during winter months, as the number and strengths of storms, i.e. atmospheric low-pressure systems, which induce ocean swells near coastlines and in this way create the primary and secondary microseismic peaks (Haubrich et al. 1963; Oliver and Page 1963; Capon 1972), vary with season and have a maximum in winter. De Becker (1990) describes how this relation can be used to forecast storm surges from Northern Atlantic low pressure systems along the Belgian coast via the monitoring of microseisms. Grevemeyer et al. (2000) use a 40-year record of microseisms recorded in Hamburg to reconstruct wave climate in the Northeast Atlantic, and in this way find indications of climate change.

At higher frequencies, starting above 1 Hz, the contrasting properties of anthropogenic noise during day and night time as well as during weekdays and weekends were investigated (Fyen 1990; Yamanaka et al. 1993; Gorbatikov et al. 2004; McNamara and Buland 2004; Bonnefoy-Claudet et al. 2006a; Guillier et al. 2007; Hanssen and Bussat 2008; Vassalo et al. 2008). Furthermore, Burtin et al. (2008) observe diurnal as well as seasonal fluctuations in ambient vibration spectral amplitudes between 2 and 15 Hz correlating with varying runoff and amount of bedload transport along a river with steep relief in the Himalayas. Similarly, Fyen (1990) finds significantly increased noise levels between 1.5 and 20 Hz at sites close to rivers related to the snow melt season and accordingly increased water flow as well as transport of large ice blocks in Norway. For the same location, Kværna (1990) describe strongly increased noise levels between 2.5 and 2.9 Hz related to increased river discharge in late spring, probably via the operation of a close-by hydroelectric power plant. De Angelis (2008) reports significant disturbance of the noise spectra between 2 and 8 Hz by strong tropical rainfall on Montserrat. Gurrola et al. (1990), Withers et al. (1996), Cara et al. (2003), Gorbatikov et al. (2004) and Mucciarelli et al. (2005) describe increased noise levels in different frequency ranges, from 0.1 up to 60 Hz, with increased wind speed. In contrast, Fyen (1990) finds no measurable effect of wind on the noise spectra between 2 and 20 Hz averaged over the individual stations of the NORESS array (radius of 1.5 km). Wilcock et al. (1999) observe the indirect effect of wind in creating high-frequency local wave noise in the oceans and on Iceland. Similarly, Vassalo et al. (2008) report a good correlation between the noise spectral amplitudes from 1.7 to 5 s and wind speed for ocean-bottom and island stations in the Campi Flegrei Caldera.

The major interest concerning repeatability in ambient vibration studies has so far been focused on the influence of varying noise sources on the stability of peak frequencies and amplitudes of single-station H/V measurements (e.g. Cara et al. 2003; Mucciarelli et al. 2003, 2005; Guillier et al. 2007). From theory, the H/V curve should depend solely on the structure below the station and not be influenced by variations in the signal source for the case of a pure Rayleigh fundamental mode wave field (Tanimoto et al. 2006), which is often assumed to describe seismic noise. In practice, though, ambient vibration measurements may contain a varying amount of other wave types, i.e. body waves, higher modes, and Love waves (Bonnefoy-Claudet et al. 2006a; Bonnefoy-Claudet et al. 2008; Köhler et al. 2007).

Guillier et al. (2007) observe stable frequencies and amplitudes only for the fundamental H/V peaks, which are located below 1 Hz for the three sites they investigate. Peaks at higher

frequencies (natural peaks) are stable in frequency but variable in amplitude, indicating their sensitivity to the position and intensity of noise sources (Bonnefoy-Claudet et al. 2006b). Parolai et al. (2004, 2005), from different studies with either repeated or long term continuous measurements, report stability in H/V frequencies with time, but not in the corresponding amplitudes, which exhibit diurnal and seasonal variations related to the ambient noise level. Besides, Mucciarelli et al. (2005) show that wind might interact directly with the sensors and wires of the recording system and thus adversely affect the H/V measurements at low frequencies.

With the increased use of array noise recordings, the influence of varying source locations and amplitudes on dispersion curves and spatial autocorrelation functions also becomes an issue. On the one hand, dominant sources within the array might distort the results for both methods (SESAME 2005). On the other hand, frequency-wavenumber (FK) analysis is based on the assumption of plane wavefronts and should work best with a single dominant source, while spatial autocorrelation (SPAC) analysis assumes that the microtremor wavefield is stochastic and stationary both in space and time (Aki 1957). In some studies, ambient seismic noise simulations have been used to investigate the reliability of the resulting data products depending on source distribution, e.g. distance between sources and array (SESAME 2005; García-Jerez et al. 2008; Roberts and Asten 2008) or isotropic versus directionally preferred distribution of sources (Cho et al. 2004; SESAME 2005; Asten 2006; Gouédard et al. 2008). Simulations by SESAME (2005) also indicate that the attenuation structure has a strong influence on measured dispersion curves, i.e. the distribution of modes in the observed wavefield, showing another way in which the source-receiver distances of the measurement configuration might influence the results.

The repeatability and temporal consistency of ambient vibration array measurements has rarely been checked for actual sites. Chávez-García et al. (2005) present array measurements at the same site for two time periods 8 years apart. However, their main motivation for the second measurement was to check the reliability of their results at low frequencies and extend the observations further in the low-frequency range. Accordingly, the second set of stations is located outside (and around) the area covered by the first array and the interstation distances and frequency bands covered by both installations simultaneously show little overlap. Cho et al. (2006a) show results for measurements with two arrays that were repeated after about three weeks, the first time under windy, the second time under windless conditions. The estimated Rayleigh wave dispersion curves can be followed to significantly lower frequencies on the windless day, which shows much less spectral contamination in the frequency range between 0.1 and 0.7 Hz. For frequencies above 0.9 Hz, however, the dispersion curves derived on both days are similar.

At a larger scale, temporal consistency of results is an important indicator of reliability and measurement uncertainty in noise cross-correlation studies for the retrieval of Green's functions and dispersion measurements from permanent broad-band stations (e.g. Bensen et al. 2007). There, an observed frequency-dependent asymmetry of the cross-correlation function has been interpreted in terms of different ambient noise sources (Stehly et al. 2006; Frank et al. 2009). While it is possible to compare results over several months or years in these cases, temporary array measurements for site characterisation are seldomly repeated at the same location or run over a sufficiently long time to investigate the consistency of results. In fact, the relatively short measurement time necessary to obtain dispersion curves is one of the main points in favour of the use of temporary array measurements for site characterisation.

Thanks to a number of international research projects targeted at gaining a better understanding of ambient vibration measurements and developing a standard technique, repeated ambient vibration recordings with small arrays, as typically used for site characterisation, are

now available from a number of sites within Europe. Here, we investigate the repeatability and consistency of three-component dispersion curve and spatial autocorrelation function estimates by analysing array data from six sites, located in Greece (Aigio, Korinthos, Lefkas, Lefkos Pirgos/Thessaloniki, Volvi) and Italy (Colfiorito). For these sites, different sets of measurements conducted by different groups in different years and different seasons with different instrumentation and array layouts are available. The sites provide a sample of different EC-8 classes, shallow to deep sedimentary layers and urban (four sites located downtown) as well as rural sites (two sites located in the countryside). Part of the measurements were conducted within the European projects NERIES (NEtwork of Research Infrastructure for European Seismology) and SESAME (Site EffectS assessment using AMbient Exciations), others resulted from the Greek-French cooperation "Accelerograph stations site characterization using ambient noise" (Savvaidis et al. 2006).

The aim of this study is to investigate stability and consistency of estimates of Love and Rayleigh wave dispersion curves as well as spatial autocorrelation curves which were measured at different times of day and in different seasons in different years, using independent installations and groups performing the field work. We do not aim to study the underlying structure of the sites in this contribution or to map the variations of the dispersion and autocorrelation curves into depth-velocity profiles. Some of the datasets used have been analysed in this respect before, and we will refer to these results and independent geotechnical information to discuss the different conditions at the individual sites. However, a detailed evaluation and inversion of the datasets to derive the shallow velocity structure is beyond the scope of this study. Mapping the dispersion and autocorrelation curves into depth-velocity profiles is a non-linear and non-unique process (depending for example on the selected model parameterisation, and generally resulting in an ensemble of models that can explain the data) and would add a new level of uncertainty compared to the direct juxtaposition of the data products (e.g. Wathelet et al. 2004, 2005, 2008; Parolai et al. 2005; Picozzi et al. 2005; Endrun et al. 2008; Schevenels et al. 2008). Moreover, the direct comparison of the measured curves enables us to judge whether the variability in the velocity models resulting from ambient vibration blind tests (Boore and Asten 2008; Cornou et al. 2009) is likely caused by problems in the measurement part or can mainly be attributed to uncertainties in the inversion part of these studies.

2 Locations and data acquisition

The locations of the individual measurement sites discussed in this study are shown in Fig. 1. Details on the data acquisition can be found in Table 1, while information on the subsurface structure at each site is listed in Table 2 and discussed in more detail below. Most of the measurements were conducted within the framework of the European research projects SESAME and NERIES. SESAME dealt with the study of the noise wavefield in general, the development of numerical tools for noise simulation, the determination of guidelines for single station and array ambient vibration measurements, and the development of software tools for ambient vibration array processing. To provide best practice recommendations, field measurements were conducted at a number of locations in Greece, Italy, Belgium and Germany (SESAME 2002a), part of which are analysed again here. For the site at Colfiorito, an analysis of the SESAME dataset has been published by Di Giulio et al. (2006). Within NERIES, subproject JRA4 "Developing and calibrating new techniques for geotechnical site characterization" in a certain sense builds upon the results of SESAME and aims at providing low-cost, efficient geophysical tools for site characterisation at the huge number of Euro-

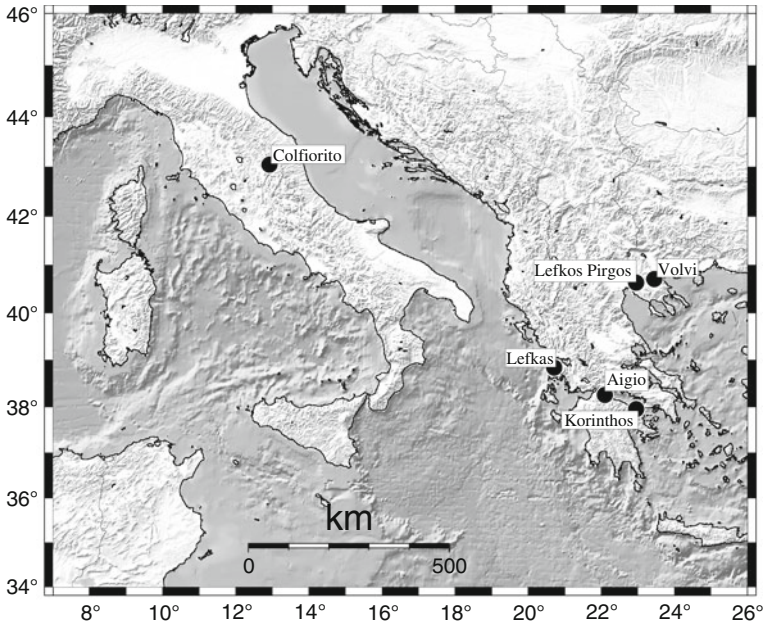

Fig. 1 Locations of the ambient vibration array measurements

pean strong motion stations. One of its tasks is on-location tests of ambient vibration array measurements. For these field tests, measurements at 20 European accelerometer sites have been performed (Endrun and Renalier 2008), a subset of which is used in this study. Further sources of data are the Greek-French Scientific Cooperation "Accelerograph stations site characterization using ambient noise" (Savvaidis et al. 2006), that conducted ambient vibration array measurements near several accelerometer sites in Greece, and a tutorial course for the sesarray software package organized by LGIT Grenoble, University Potsdam and ITSAK Thessaloniki that took place in Thessaloniki, Greece, in December 2008.

With the exception of the site Lefkos Pirgos, all measurements employed the same type of seismometer (Lennartz sensor's Le3D), whereas various digitizers and sampling rates were used (Table 1). The acquisition was done by different field teams, with some overlap in the persons involved. Typical measurement times cover the whole day, with more measurements conducted in the afternoon, while the SESAME experiment at Colfiorito was done mainly during night time. Acquisition time for each individual array varies between 30 minutes and 2 h for different teams performing the measurements, and while the array layout is mainly circular with a central station for the NERIES and Greek/French measurements, other layouts were used in the SESAME experiments (Fig. 2). The season during which the experiments were conducted ranges from early spring (NERIES measurements at Colfiorito) via midsummer (SESAME measurements in general) to winter (sesarray course at Lefkos Pirgos). The time elapsed between the repetitions of the measurements lies between two years (Aigio and Korinthos) and more than 6 years (Lefkos Pirgos). The site locations range from urban to rural and are described in more detail below.

The sites of Aigio and Korinthos are both located in towns at the southern shoreline of the Gulf of Corinth, a Quarternary graben-type structure which is actively extending in North-South-direction by 5–20 mm/a (Nyst and Thatcher 2004). The graben is antisymmet-

Table 1 Acquisition parameters for repeated measurements

Experiment	Time	# Arrays $d_{min,\,max}$ [m]	# Stations	Duration [min]	Sensors/ digitizers	Sampling rate [Hz]
Aigio						
Greek/ French	11/05/2005, afternoon	3 10, 78	6	30–60	Le3D (5s)/ CityShark II	125
NERIES	09/17/2007, whole day	3 3,70	8	100–150	Le3D (5s)/ EarthData	200
Colfiorito						
SESAME (Arr. E)	07/30+ 07/31/2002, evening to morning	1 30, 235	12	900	Le3D (5s)/ MarsLite	125
NERIES	03/30/2008, afternoon	3 14, 183	8	45–55	Le3D (5s)/ EarthData	100
Korinthos						
Greek/French	11/07/2005, evening	3 7, 60.5	6	30–40	Le3D (5s), CityShark II	200
NERIES	09/18/2007, whole day	4 4,142	8	50–85	Le3D (5s), EarthData	100
Lefkas						
SESAME	08/03/2002, around noon	1 20, 199	13	190	Le3D (5s)/ MarsLite	125
Greek/ French	11/02/2005, evening	3 13, 117	6	30-59	Le3D (5s)/ CityShark II	200
Lekos Pirgos (Thessaloniki)						
SESAME	08/06/2002, evening	1 48, 409	13	120	Le3D (5s)/ MarsLite	125
Sesarray course	12/09/2008, around noon	3 3.5, 374	10	35-55	Guralp CMG6-T	100
Volvi						
SESAME	08/08/2002, whole day	3 21, 526	13	65-120	Le3D (5s)/ MarsLite	125
NERIES	09/22/2007, whole day	4 9, 931	8	50-80	Le3D (5s), EarthData	100

Arrays specifies the number of arrays (with increasing diameter) consecutively deployed at a single location during an individual measurement campaign. The smallest and largest interstation distances realized at each location, d_{min} and d_{max}, are also reported. # stations gives the number of stations used in each of these arrays. The duration refers to the time each of these arrays was continuously recording, while the time of the experiment describes the time range during which all the individual array measurements took place

ric, with a rising Southern and a subsiding Northern coast (Pham et al. 2000). Accordingly, the Southern shoreline is formed by normal faults dipping at 40–50° towards the rift (King et al. 1985) and showing a well-developed en echelon system (Tiberi et al. 2000). Individual fault blocks are covered by thick Plio-Quarternary sediments incorporating lacustrine, coastal plain, fluvial and alluvial fan deposits (Doutsos and Poulimenos 1992). The basement around the Gulf consists of a West-verging stack of flat-lying nappes belonging to the Hellenides, each of the nappes including a 2–3 km thick competent series of Mesozoic carbonates covered by a thinner incompetent layer of flysch (Doutsos and Poulimenos 1992). At Aigio, the top-most sedimentary layer consists of Holocene sands and clays of about

Table 2 Site characteristics from geotechnical measurements, as far as available, for the six sites

site	v_0[m/s]	v_S[m/s]	v_{bd}[m/s]	d_{bd}[m]	Z_m	Reference
Aigio	190	430	1200	20	3.5	Athanasopoulos et al. (1999)
Colfiorito	144	160	977	61	7.6	Di Giulio et al. (2006)
Korinthos	270	–	–	–	–	Picozzi et al. (2007)
Lefkas	110	110	600	8	6.3	Triantafyllidis et al. (2006)
Lefkos Pirgos	240	530	2300	150	5.4	Anastasiadis et al. (2001)
Volvi	100	430	2600	196	7.6	Raptakis et al. (1999)

v_0 refers to the S-velocity at the surface, v_S to the average S-velocity of the sediment layers, and v_{bd} to the bed-rock S-velocity. d_{bd} gives the depth to the bedrock (thickness of the sedimentary layers), and Z_m the average impedance contrast across the sediment-bedrock interface. Z_m is calculated using the average sedimentary S-velocity and—with the exception of Lefkas—fixed values of 2, 000 kg/m^3 and 2, 500kg/m^3 for the average density of the sediments and of the bedrock, respectively. For Lefkas, density values were available from the reference (1, 900kg/m^3 for the sediments and 2, 200kg/m^3 for the bedrock) and applied accordingly. The last column gives the reference for the used velocity model. Information for Korinthos is sparse, as the corresponding borehole (to a depth of 40 m) did not reach the bedrock

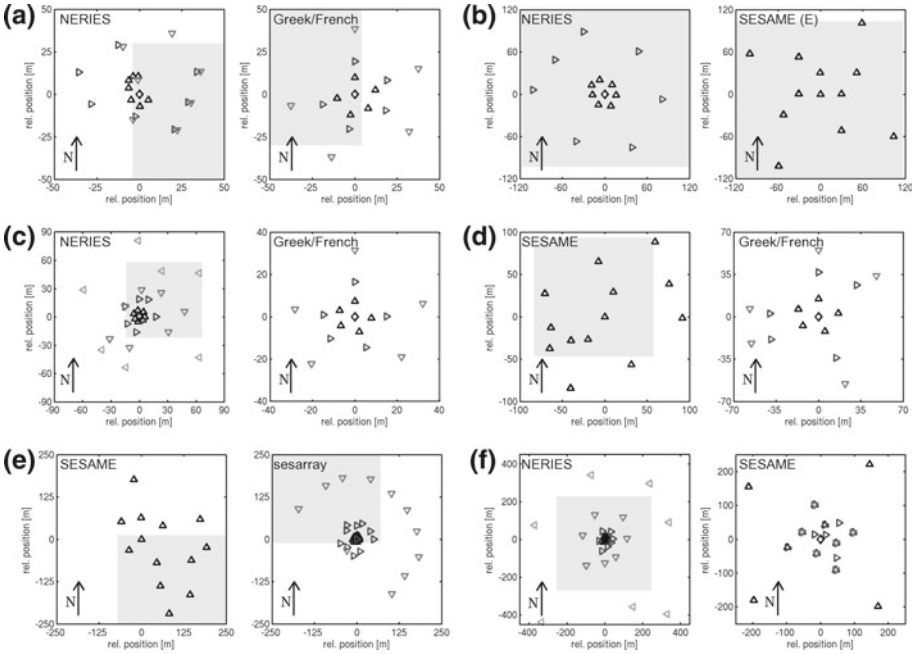

Fig. 2 Array layouts deployed during the repeated measurements. *Triangles of different colors and orientations* represent seismometer positions belonging to one individual array. For circular arrays, the central station which stays fixed for arrays with different diameters is marked by a *black diamond*. *Gray shaded boxes* outline the location of the two measurements at the same location relative to one another. For repeated measurement with arrays of different sizes and similar locations, only the position of the smaller array with respect to the larger one is indicated. **a** Array deployments at Aigio. **b** Array deployments at Colfiorito. **c** Array deployments at Korinthos. **d** Array deployments at Lefkas. **e** Array deployments at Lefkos Pirgos (Thessaloniki). **f** Array deployments at Volvi

20 m thickness ($v_S < 500$ m/s) overlying Pleistocene and Pliocene conglomerates and marls ($v_S > 1,000$ m/s) above the limestone basement at about 120 m depth (Athanasopoulos et al. 1999). At Korinthos, the morphology as well as the bedrock depth are less well known. Slow sediments ($v_S < 600$ m/s) extend to at least 40 m depth. Both array sites were located within the towns. In Aigio, stations were installed in a park and on a neighbouring square, with the cliff facing towards the Gulf of Corinth directly North of the recording sites. Noise sources include pedestrians walking next to the stations as well as car traffic on close-by roads. In Korinthos, the stations were installed on and around a large town square, with a lot of pedestrian traffic during the morning. The square is bounded to the North–Northwest by a large and busy road (compare Fig. 5). The array configurations used at Aigio and Korinthos are shown in Fig. 2a and c.

The site at Colfiorito is located within a 3 km wide intramountain basin at a height of ~700 m above sea level in the southern part of the Apennine arc. This structural depression is filled with Quarternary alluvial deposits composed of lateral debris fans interfingering with lacustrine sandy-clayey deposits that constitute the main body of the fill ($v_S < 200$ m/s). The basement below these soft sediments consists of limestone and marl rocks (v_S around 1,000 m/s) of the Umbria–Marche Meso–Cenozoic sequence (Di Giulio et al. 2006). The sediment-basement interface has been mapped by Di Giulio et al. (2003) and shows a very irregular topography, containing narrow sub-basins with sedimentary thicknesses of up to 180 m. These complex lateral variations have been attributed to recent karstic or tectonic (normal-faulting) activity (Di Giulio et al. 2003). The bedrock is located between 55 and 70 m depth at the measurement location. Measurements took place in a rural environment on the premises of a farm ~2 km to the North-East of the village of Colfiorito, with no cultural noise sources in the form of industrial activity or pedestrians in the vicinity. However, the state highway SS77, which is one of a limited number of East-West connections through the Apennines, takes a bend around the valley ~1.5 km to the North-West of the array locations. The array configurations used are depicted in Fig. 2b.

The site at Lefkas is located on the Ionian island of the same name, within the town at its North-Eastern corner that is situated on a peninsular extending into the sea at 1–5 m above sea-level. The town is almost completely underlain by Holocene shallow alluvial and lagoon deposits (v_S = 100–150 m/s) of low rigidity and resistance (Drouet et al. 2008; Kassaras et al. 2008). The thickness of this formation, which overlies a stiff marl ($v_S = 600$ m/s), is variable beneath the town, from 16 m in the town center to zero (marl outcropping) at its southern boundary, implying a trough-shape (Kassaras et al. 2008). The variable layering of sands and clays within these soft shallow deposits, covered by human in-fill, caused liquefaction during the August 2003 earthquake ($M_w = 6.2$). Due to the particular urban environment at this site, the array stations had to be installed on parking lots and at the side of roads within the town centre. The area covered by the arrays is situated between two permanent accelerograph stations showing significant differences in their respective site response characteristics, attesting to lateral heterogeneity. The array layouts deployed in Lefkas are shown in Fig. 2d.

The site of Lefkos Pirgos is located within the city of Thessaloniki, with more than a million inhabitants the second largest town in Greece, next to the sixteenth century Ottoman monument of the same name ("White Tower"). The town of Thessaloniki with its suburbs extends along the Thermaikos Gulf coastal zone, from sea level to an altitude of about 100–150 m towards the East-Northeast. It is situated on three large-scale geological structures, which are oriented in the Northwest-Southeast direction, with an increasing thickness of the sedimentary cover towards the coast (West-Southwest direction) (Anastasiadis et al. 2001): The surficial formation consists of recent soft deposits of Holocene clays, sands and pebbles

(v_S = 200–350 m/s) with a thickness of about 30 m at the measurement location. It is underlain by alluvial deposits, largely belonging to the red silty clay series (v_S = 350–850 m/s), and mainly dating from the Neogene period. This formation extends to about 150 m depth at the location of the measurements (Triantafyllidis et al. 2001) and is underlain by the bedrock consisting of gneisses, epigneisses and green schists (v_S = 1,750–2,500 m/s). The measurements took place next to the seashore (fortified sea front and harbour) and the waterfront boulevard, which are local sources of noise (compare Fig. 5). The shapes of the arrays realized at Lefkos Pirgos are shown in Fig. 2e.

The site at Volvi is the subject of numerous studies as it has been declared a European test site for site response estimations (e.g. Jongmans et al. 1998; Pitilakis et al. 1999; Chávez-García et al. 2000; Raptakis et al. 2000; Savvaidis et al. 2000). It is located in the Volvi graben, a part of the Mygdonian basin, between Lake Langhadia and Lake Volvi East-Northeast of Thessaloniki. The graben is actively extending in a North-South direction at a rate of about 5.7 mm/a (Martinod et al. 1997). It is filled by sediments of the Mygdonian (fluviolacustrine, deltaic, lacustrine, lagoonal and estuarine deposits; v_S = 150–450 m/s) and Promygdonian (conglomerates, sandstones, silt-sand sediments and red-beds; v_S = 650–800 m/s) systems, which are offset along two faults near each shoulder of the graben, on top of crystalline gneiss (v_S = 2,600 m/s; Pitilakis et al. 1999; Raptakis et al. 2005). Measurements were carried out in the centre of the valley between the two lakes, where the sediment-basement interface shallows compared to the area of the lakes to around 196 m depth. The location is in a rural area, without any major roads, industrial activity, pedestrians or other known sources of noise in the vicinity. 3 km North of the array, though, the Egnatia Motorway, which was still under construction during the first measurement in 2002, crosses Volvi valley in a East-West direction (compare Fig. 5). The array layouts deployed at Volvi are shown in Fig. 2f.

3 Methods

Two different processing techniques for obtaining surface wave phase velocities are generally used in the array analysis of ambient vibration measurements, the FK method and the SPAC method (Okada 2003). The capabilities of both methods have recently been investigated and compared for synthetic ambient vibration data in a simple layer-over-a-halfspace case by Wathelet et al. (2008).

The FK method can be divided into two subgroups, the beamforming (conventional) FK method (Lacoss et al. 1969) and the high-resolution FK (Capon 1969). Both assume that the signal is propagating across an array of sensors in the form of plane waves. If, at a given frequency, the horizontal wavenumbers (corresponding to the azimuth and velocity of a plane wave propagation across the array) are known, the output of the array can be optimized by calculating the relative arrival times at all sensor locations, shifting the signals according to these delay times, and stacking. As the propagation direction and velocity are usually not known in advance, stacking is performed on a dense wavenumber grid for each frequency. The maximum of beampower found on this grid gives an estimate of the propagation direction and velocity of the plane wave. The high-resolution FK was introduced by Capon (1969) as an improvement to this method. This technique adds weights to each sensor's contribution to the array output, which are calculated so as to minimize the energy at wavenumbers other than the considered one. Thus, the capability to distinguish between two waves travelling at close wavenumbers is improved and the resolving power increased.

The SPAC method was originally introduced by Aki (1957) for vertical recordings of circular arrays with a central station. It is based on the assumption that the noise wavefield

is random and stationary in both space and time. Under these conditions, the azimuthally averaged vertical component spatial autocorrelation $\overline{\rho}_V$ between the stations along the circle and the one at its centre can be expressed in terms of a Bessel function J_0 of the first kind of zero order:

$$\bar{\rho}_V(f,r) = J_0\left(\frac{2\pi f r}{c_R(f)}\right) \tag{1}$$

The argument of the Bessel function is given by a ratio that, besides the investigated frequency f and the radius of the circle r, contains the desired Rayleigh phase velocities $c_R(f)$. Accordingly, the Bessel functions can first be derived by correlating the seismic traces between station pairs and averaging over azimuthal directions. In a second step, they may either be inverted to determine the phase velocity curve (which is then subjected to another non-linear inversion procedure), or used directly to constrain the velocity distribution with depth (Asten et al. 2004; Wathelet et al. 2005; Asten 2006). A number of advances have been made to lessen the strong constraints on station distribution inherent to the original version of SPAC. Among these are the extended spatial autocorrelation method [ESAC (Ohori et al. 2002)], the centreless circular array method [CCA (Cho et al. 2006a)], and the modified spatial autocorrelation method [MSPAC (Bettig et al. 2001)]. The MSPAC method allows the use of stations distributed on imperfect circles (for example due to obstacles like houses and roads when measuring within towns) by substituting the single radius in Eq. 1 by an integral over rings of a limited radial range. A further improvement is the extension of the MSPAC method to all three components of the recordings, allowing for the determination of the Love wave dispersion curve and the relative amount of Rayleigh and Love wave contributions to the ambient vibration wavefield (Köhler et al. 2007). The radial component $\overline{\rho}_R$ and the transverse component $\overline{\rho}_T$ of the azimuthally averaged spatial autocorrelation can be expressed as a combination of Bessel functions of the first kind of the orders zero and two with arguments similar to Eq. 1, but containing either Rayleigh phase velocity $c_R(f)$ or Love phase velocity $c_L(f)$, and weighted against one another using a coefficient $\alpha(f)$ that describes their frequency-dependent relative contributions to the wave field. Similar to Eq. 1, the formulas are given here only for the case of a single fixed array radius (Bettig et al. 2001). Their generalisation to the case of an imperfect circular array by integration over a limited radial range can be found in Köhler et al. 2007.

$$\begin{aligned}\bar{\rho}_R(f,r) = {} & \alpha(f)\times\left\{J_0\left(\frac{2\pi f r}{c_R(f)}\right) - J_2\left(\frac{2\pi f r}{c_R(f)}\right)\right\} \\ & + (1-\alpha(f))\times\left\{J_0\left(\frac{2\pi f r}{c_L(f)}\right) + J_2\left(\frac{2\pi f r}{c_L(f)}\right)\right\}\end{aligned} \tag{2}$$

$$\begin{aligned}\bar{\rho}_T(f,r) = {} & \alpha(f)\times\left\{J_0\left(\frac{2\pi f r}{c_R(f)}\right) + J_2\left(\frac{2\pi f r}{c_R(f)}\right)\right\} \\ & + (1-\alpha(f))\times\left\{J_0\left(\frac{2\pi f r}{c_L(f)}\right) - J_2\left(\frac{2\pi f r}{c_L(f)}\right)\right\}\end{aligned} \tag{3}$$

With the help of the Rayleigh wave information determined from the vertical component by Eq. 1, the Love wave phase velocity and α can be extracted from Eq. 2 and 3.

Other improvements to the SPAC method include the multiple mode spatial autocorrelation method [MMSPAC (Asten et al. 2004)], which involves the simultaneous direct inversion of several SPAC curves measured for different array radii. Fitting the curves over multiple maxima and minima improves the resulting estimates of shear-wave velocities, including the resolution of near-surface low-velocity layers, as well as the recognition of higher

mode wave propagation in the SPAC curves (Roberts and Asten 2005; Asten 2006, 2009). Cho et al. (2006b) and Tada et al. (2007) have formulated a general theory for circular array measurements of ambient vibrations based on ratios between different types of spectral densities of Fourier expansions of the set of records with azimuth. Other methods rely on the equivalence of azimuthal averaging by either distributing stations in various azimuths on a circle or using a pair of only two stations, but with recordings of a sufficient duration to assume azimuthally evenly distributed sources (e.g. Chávez-García et al. 2005, 2006).

In the analysis of our array datasets, both the conventional and the high-resolution FK were applied to the three-component recordings of each array to determine a branch of the Rayleigh as well as Love wave dispersion curves. Traditionally, only the vertical component of ground motion recordings is used to derive Rayleigh wave dispersion curves. An application using all three components to additionally determine the dispersion of Love waves was given by Fäh et al. (2008). To isolate Love from Rayleigh waves on the horizontal components, they are rotated into a radial and a transverse component for each individual time window and each frequency band by regarding each azimuth on the horizontal wavenumber grid as corresponding propagation direction. Naturally, this strategy can work only if each time window in each frequency band contains energy from only one main source direction and if sources are the same for Love and Rayleigh waves. These constraints result in an incomplete separation of Rayleigh from Love waves on the horizontal components for some field datasets, especially when using the high-resolution FK. However, with the aid of the Rayleigh wave dispersion measured on the vertical component, Love wave dispersion curves could be reliably derived in all cases.

For some measurements, i.e. the ones conducted during SESAME at Colfiorito, Lefkas and Lefkos Pirgos, data were recorded with one large array consisting of a large number of stations and featuring variable, small as well as large, interstation distances. For the NERIES measurements, less stations were available. But instead, data were accessible in near-real time through communication by a wireless mobile ad-hoc network between stations in the field (Ohrnberger et al. 2006). Having data readily at hand allows for preliminary in-field processing. A data-adaptive concept was used in the design of consecutive arrays, based on the already available partial dispersion curve branches from near-real time processing. This concept helps to determine the dispersion curve within overlapping frequency bands to increasingly longer periods from one array to the next.

Curves from the individual arrays at each site and from both conventional and high-resolution FK were combined to yield a single dispersion curve across a broad frequency range. Conventional and high-resolution FK give very similar dispersion curves in all cases, while the high-resolution FK shows some potential to enlarge the usable frequency range to longer periods, as was also observed by Wathelet et al. (2008) for a synthetic case. The well-resolved frequency range for FK processing with each array is derived from the array response function, as described by Wathelet et al. (2008) and Cornou et al. (2009).

In addition to the FK techniques, the SPAC method was applied in the form of the three-component MSPAC (Köhler et al. 2007). Autocorrelation functions were computed for the vertical as well as transverse and radial components, averaging across five or more station pairs with comparable interstation distances and variable azimuths. Then, a grid search can be conducted across velocities and frequencies for all three components of the SPAC functions and various interstation distances. It results in the simultaneous determination of Rayleigh and Love wave dispersion curves and the coefficient α indicating the relative Rayleigh and Love wave contributions to the wavefield. However, in the following we mainly choose to directly compare the three components of the SPAC functions between repeated measurements at the same location. Data products derived from them, e.g. dispersion curves, give

rise to additional uncertainties because of the inverse problem solution necessary to obtain them (Asten 2009). The SPAC functions are usually displayed covering a broad frequency range for each individual ring used in azimuthal averaging. Due to the variable array layouts deployed by the different groups performing the repeated measurements, however, similar ring radii were seldom, and only by chance, available for comparison. So instead, the SPAC functions are displayed for single frequencies and covering all available ring radii (Ohori et al. 2002), which is an equivalent representation according to Eq. 1.

4 Results

4.1 Amplitude spectra

To test the stability and consistency of the ambient vibration wavefield from one measurement to another at the same location, we compare average properties of the wavefield from repeated measurements. The first of these properties are amplitude spectra, which show the energy content and distribution with frequency. The variability of spectra reflects changes in the wavefield composition. Its analysis is therefore essential for the interpretation of variations in dispersion curves. In the following, three examples are discussed in detail—one from a relatively calm and unproblematic urban location, Korinthos, one from a more noisy and complex urban location, Lefkos Pirgos in Thessaloniki, and one from a rural location in the same area, Volvi.

Figure 3 shows the spectral variations at the central station of each deployment within an individual measurement cycle for the three locations. In each of the three cases, the experiment with the longest recordings for the central station is displayed, which means that for Korinthos and Volvi, the analysed data were obtained during the NERIES measurements, while for Lefkos Pirgos data from the SESAME experiment are used. For Korinthos, the four array deployments of various sizes were carried out between 09:00 am and 04:30 pm. For Volvi, the complete time range covered by the four deployments lies between 09:40 am

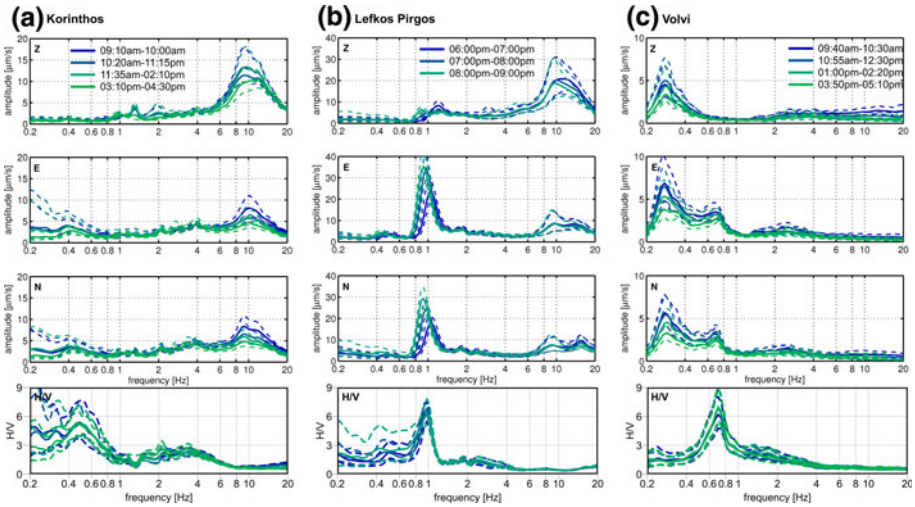

Fig. 3 Three-component amplitude spectra and H/V spectral ratios of the central array station at three sites averaged over different time windows (*solid lines*). *Dashed lines* indicate standard deviations

and 05:00 pm. For Lefkos Pirgos, the analysed data are from continuous recordings, which were available at the central station for 3 h and split into three equal time windows between 06:00 pm and 09:00 pm. In addition to the amplitude spectra, H/V spectral ratios (Nakamura 1989) are also presented.

Spectra from the three sites show different shapes and amplitudes. The urban sites both have broad spectral maxima between 8 and 15 Hz on all three components, caused by anthropogenic sources (traffic, machinery, pedestrians; e.g. McNamara and Buland 2004). Lefkos Pirgos shows an additional peak, especially on the horizontal components, around 1 Hz, while the main peak at the rural site of Volvi is located at 0.27 Hz with much reduced amplitudes for all higher frequencies. This peak is a manifestation of the secondary microseismic peak, which is caused by interaction of oceanic waves. A peak below 0.5 Hz is also observed at the urban sites, but due to its small amplitudes (around 5 μm/s) does not appear as prominently on the recordings of Korinthos and Lefkos Pirgos. Similarly to Volvi, this peak shows larger amplitude on the horizontal than on the vertical component. The well-defined microseismic peak in the measurements from Volvi is explained by comparison with weather data (ECMWF ERA-interim dataset, available at http://data-portal.ec\discretionary-mwf.int). They show a prominent low-pressure system over the Northern Atlantic South-West of Iceland on the day the measurements were conducted, which is absent during the measurements at Korinthos and Lefkos Pirgos. Storms associated with low-pressure systems over the Northern Atlantic and Pacific are known to increase the amplitude of microseisms in the Northern hemisphere during fall and winter (e.g. Capon 1972; Cessaro 1994; McNamara and Buland 2004; Stehly et al. 2006), in such a way that an increase in microseismic activity can even be used to predict storm surges (De Becker 1990). Variations in closer environmental sources, i.e. associated with wave action in the northern Aegean, could also influence the low-frequency part of the spectra at Volvi. For these sources, no data are available for comparison, though. Likewise, the horizontal component peak around 1 Hz at Lefkos Pirgos can be related to waves, i.e. the direct interaction of the sea with the harbour walls of Thessaloniki South-West of the array location, or to anthropogenic sources, as in this frequency band both natural and cultural sources are active (Bonnefoy-Claudet et al. 2006a).

Comparison of the spectra for different time windows shows that, though spectral shapes remain similar throughout the day, spectral amplitudes do vary. For both, the rural site of Volvi and the urban site of Korinthos, amplitudes of all three components decrease with time, by an average amount of 35% from morning to afternoon. At Lefkos Pirgos, the picture is different, though: Here, amplitudes on the horizontal components increase by an amount of about 35% with time from afternoon to early evening. Besides, the main amplitude peak on the horizontal components shifts in frequency, from 1.07 to 0.92 Hz. The vertical component shows less amplitude variations, though the shape of the small peak around 1 Hz also varies with time. In contrast, and as reported in various other studies (e.g. Parolai et al. 2004; Panou et al. 2005; Guillier et al. 2007), the shape and amplitude of the H/V curves remains fairly constant.

Additionally, the shape of the spectra can change considerably between repeated measurements (Fig. 4), which is illustrated for Volvi and Lefkos Pirgos, a rural and a very urban site in the same area. For example, in Volvi, the three components of the amplitude spectrum show an additional maximum between 1.5 and 5 Hz for the SESAME measurements, with almost double amplitudes around 3 Hz, that was not observed during the NERIES experiment, even though the location of the central station was the same for both deployments within 23 m and the time of day of the recordings is about the same. This additional peak can be explained by an additional man-made source near the array, for example due to work on the fields around the test site. This explanation is in keeping with the fact that the SESAME

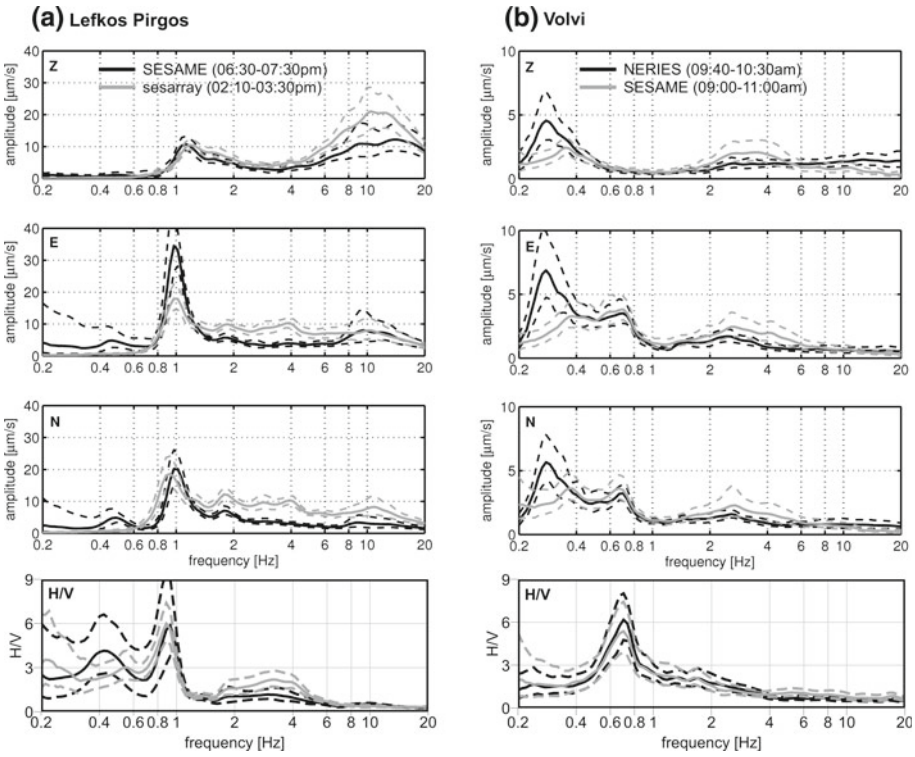

Fig. 4 Comparison of three-component amplitude spectra and the H/V spectral ratios between the two repeated measurements for two sites. As in Fig. 3, *solid lines* indicate average spectra (spectral ratios, respectively) and *dashed lines* their standard deviations

measurements were done on a workday (Thursday), while the NERIES experiment was conducted at the weekend (Saturday). In addition, the main low-frequency peak, which is observed at 0.27 Hz in the NERIES data, is not observed during the SESAME measurements. Here, the high amplitudes at low frequencies terminate at around 0.35 Hz, a frequency that is more in keeping with the higher peak frequencies observed in Korinthos and Lefkas Pirgos (Fig. 3). The different visibility of the microseismic peak can be explained by different, and stronger, storm activity during the NERIES measurements.

At Lefkos Pirgos, no recordings were made during similar time windows. The spectra are compared between the closest stations of the two layouts, at a distance of 35 m, which are the South-Eastern station of the SESAME deployment and the North-Western station of the medium-sized sesarray array. Comparing the spectra, the broad high-frequency maximum around 12 Hz on the vertical component has a twice as large amplitude for the sesarray measurements than for the SESAME data. Besides, amplitudes on the horizontal components are also more than twice as large between 1.5 and 8 Hz for the sesarray measurements. Together, these observations point to stronger background activity during this measurement, which is probably both anthropogenic as well as meteorological. Around the low-frequency peak around 1 Hz, on the contrary, the horizontal amplitudes of the sesarray spectra are smaller, most significantly on the East component of the recordings. Interestingly, the low-frequency peak is observed at different frequencies on both horizontal components during the sesarray recording. If the source is indeed the waves running against the harbour wall, the different

frequencies could indicate different wave resonances within the harbour, which has a somewhat larger North-South than East-West extension near the measurement location.

Again, H/V spectral ratios show a fairly constant behaviour—at least at frequencies down to the lower flank of the main peak—for both measurements. The amplitude of the main peak varies slightly for both measurements at Volvi, which might be caused by a different amount of Love waves present in the wavefield.

Together, these observations show that, already during the limited time range of each measurement, changes in the spectral amplitudes and, sometimes, shapes do occur, while spectral shapes might vary widely between measurements conducted on different days and in different years. This has also been observed during longer-term deployments of single stations for H/V measurements (Parolai et al. 2004; Panou et al. 2005; Guillier et al. 2007). Nevertheless, consistent with the findings in this study, the derived H/V peak frequencies are reported to be stable with time. However, no investigation has yet been conducted of the influence of the spectral variability on dispersion curve measurements with ambient vibrations arrays.

4.2 Location of main ambient vibration sources

In addition to the stability of amplitude spectra, the stability of the ambient vibration sources as derived from FK analysis between the first and second measurement at the different locations has been investigated. During conventional FK analysis, the records of each array are split into time windows of 50*T, overlapping by 5%, where T is the central period of each frequency band considered. FK analysis is carried out for each of these time window and the azimuth and slowness of the position of maximum energy in the wavenumber plane is stored. Figure 5 shows the distribution of these slowness values from all individual time windows for the vertical component FK for the two independent experiments conducted at Korinthos, Lefkos Pirgos and Volvi, respectively. The frequency bands shown were selected in order to illustrate variations over the complete analyzable bandwidth. For each location, the selected frequency band was determined by the resolving capabilities of individual arrays in each deployment. It is apparent that the azimuthal location of the main sources that contribute to the ambient vibration wavefield changes between the two measurements at each site, for urban sites as well as for the rural site. Some of the sources can be identified, taking into account the array locations and the imaged azimuthal distribution (Fig. 5).

The location of sources can most easily be explained in the case of Volvi: During both measurements, a large part of the energy in the frequency band between 1.5 and 2.2 Hz is coming from the area between 110°and 180°. In this azimuth from the array, the Thessaloniki-Kavalas road at the southern boundary of Volvi valley crosses the village of Stivos. The village, which, at a distance of about 1.6 km to the centre of the arrays, is the settlement closest to the measurement site, as well as traffic entering and leaving this road, act as noise sources. During the SESAME measurement, another isolated source of noise is found in the direction of the village of Nymfopetra, while during the NERIES measurements, a well defined source is found at a direction of ∼300°. It might be related to the village of Scholario as well as the Egnatia Motorway, which has a junction with on-ramps, exits and bridges to enter and leave the highway in this direction at about 3.4 km distance from the centre of the arrays. The junction leads to locally increased as well as accelerating and decelerating traffic that, together with movement of cars over the bridges, provides a significant source of noise. The motorway's construction started in 2000, and while the part North of Thessaloniki in Volvi valley was ready and in use during the NERIES measurements in 2007, it was still under construction and not open to traffic during the SESAME measurements in August

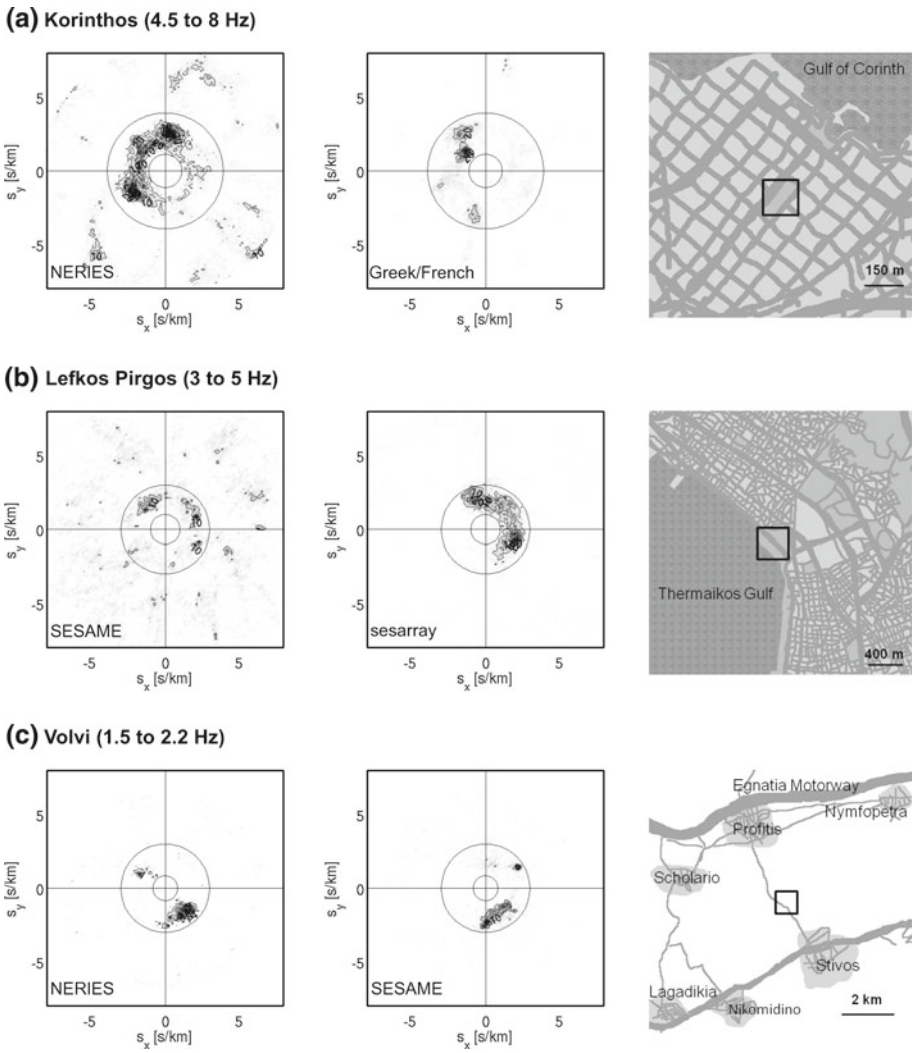

Fig. 5 Slowness distribution, determined by FK analysis, of the main contributing energy on the vertical component within specific frequency bands for two experiments at each of the three sites (*left and center column*). The corresponding Rayleigh wave dispersion curves can be found in Figs. 6 and 7 and the *two circles* on *each plot* indicate the maximum and minimum slowness of the measured dispersion curves in the considered frequency windows. For comparison with possible noise sources, schematic maps of the array locations are shown in the *right column*, where *black rectangles* outline the approximate location of the array deployments

2002, which means that the junction was not yet available as a source. This is consistent with our observations.

For Lefkos Pirgos, the recordings of the sesarray course show energy contributions from a broad azimuthal range, between 320° and 170°, for frequencies between 3 and 5 Hz. These sources are clearly located in the city of Thessaloniki and show a good correlation with the course of several major roads, which follow the Thermaikos Gulf by taking a turn from North-West to South on the land side of the arrays. During the SESAME recordings, the dis-

tribution of sources looks more scattered and might be more focused on individual crossroads or bends in the roads.

During the NERIES measurements at Korinthos, sources—probably associated with traffic—can be found almost all around the array in the frequency range of 4.5–8 Hz, though locations between 200° and 30° dominate. This is in agreement with the course of the largest and most busy road North of the square were the measurements took place. The strongest maxima at about 10° and 225° might be related to the crossroads at the North-West and South-West corners of the square. The Greek-French measurements, which were concentrated more in the North-East part of the square (Fig. 2) shows a different picture with only a few well-defined concentration of energy around 190°, 300° and 340° in the considered frequency range. They could be related to individual crossroads or construction sites around the area where the measurements took place.

4.3 Dispersion curves

Figure 6 shows all Rayleigh and Love wave dispersion curves determined at the site of Volvi. All dispersion curves from FK analysis shown in the following represent a combination of the results for all arrays deployed during each measurement at each locations and the analysis with conventional as well as high-resolution FK. Dispersion curves can be determined over a broad frequency range, from 0.3 Hz up to 30 Hz for the NERIES Rayleigh wave data. The high-frequency limit extends to considerably higher frequencies here than in the case of the SESAME data due to the significantly smaller interstation distance of the smallest NERIES array (Table 1). The reliable frequency range for the determination of dispersion curves by FK was derived from the analysis for the respective array response functions (Wathelet et al. 2008). Within these limits, an excellent agreement is observed for both wave types between the results derived by FK analysis and by SPAC for each individual experiment, on the one

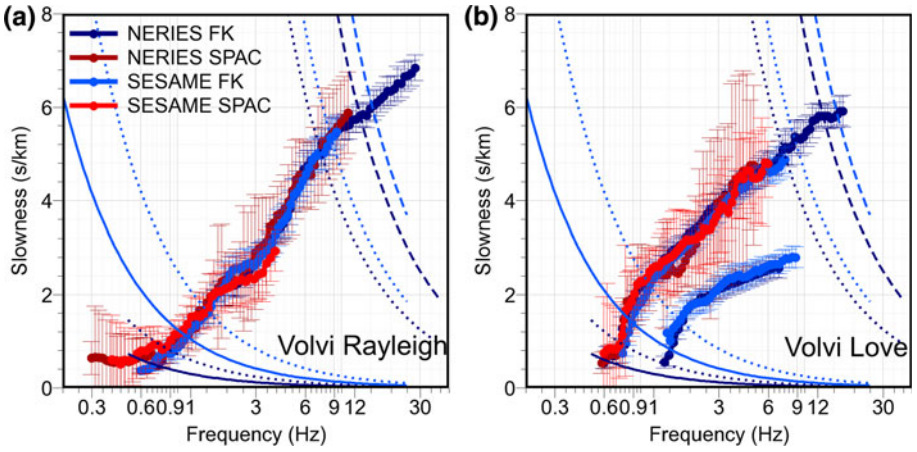

Fig. 6 **a** Comparison of Rayleigh wave dispersion curves derived from ambient vibration data recorded at Volvi during different measurements (NERIES and SESAME) and using different methods of analysis (FK and SPAC). Constant-wavenumber lines outline the upper and lower resolution limits (Wathelet et al. 2008) of the correspondingly colored FK curves (*solid* $k_{min}/2$, *dashed* k_{min} and k_{max}, *dotted* $k_{max}/2$; where $k_{min}/2$ is the radius of the central peak of the array response function at mid-height and k_{max} is the minimum wavenumber at which this amplitude is reached again outside of the central peak) **b** same as **a** for Love waves, where a higher mode is consistently observed in addition to the fundamental mode

hand, as well as between results from both of the measurements on the other hand. A Love wave higher mode is consistently identified from FK analysis of both datasets. The dispersion curves derived from SPAC show significantly larger uncertainties than the FK data. The uncertainties are in this case directly determined from the gradient of the misfit function at each frequency around the optimum slowness determined by the grid search. In contrast, the uncertainties shown for the FK curves correspond to standard deviations derived from the edited distributions of slowness values from all analysed time windows at each frequency, which are close to Gaussian in shape. It is also apparent that outside the lower limit of the reliable frequency range, the dispersion curves determined by FK systematically deviate to lower slownesses, and thus higher phase velocities, compared to the dispersion curves derived from SPAC. This observation is similar to what was found in a recent synthetic test (Wathelet et al. 2008) and in applications of different variants of the SPAC method (Cho et al. 2004; Köhler et al. 2007). It can be explained by the different factors that limit resolution for the FK and SPAC methods, respectively (Asten and Boore 2005). For FK methods, resolution at low frequencies is limited by the inability to separate between different wave components (which implies that resolution at low frequencies can be improved by the high-resolution FK, as is indeed observed in our datasets). Smeared azimuthal distributions of wave energy due to limited resolution lead to average estimates of wavenumber which are biased to shorter wavenumbers, i.e. higher velocities (Asten and Boore 2005; Claprood and Asten 2009). SPAC methods, on the contrary, do not aim at the resolution of individual wave components, but perform an azimuthal averaging of wave energy. Rather, their low frequency resolution limit depends on the mutual coherence of the recordings at different stations (Cho et al. 2004) and accordingly, they are more susceptible to incoherent noise which will bias the coherency, and the velocity estimates, to lower values (Asten and Boore 2005). Still, they can potentially resolve the dispersion curves to lower frequencies than FK methods (Claprood and Asten 2009).

For the five other sites, a similarly good agreement between the dispersion curves derived by FK and by SPAC is observed for each individual measurement. Comparisons between the repeated measurements are depicted individually for Rayleigh and Love wave dispersion curves derived from FK analysis (Figs. 7 and 8). Here, the dispersion curves from FK are only shown between the upper and lower resolution limits as determined from the corresponding array responses.

For all sites, the agreement between the Rayleigh wave dispersion curves is excellent in the frequency part covered by both measurements (Fig. 7). At Aigio, Rayleigh wave dispersion can be measured up to 45 Hz (which is close to the Nyquist limit for the employed sampling frequency of 100 Hz) and in Korinthos, up to 30 Hz from the NERIES data, whereas for the other locations and experiments, the dispersion curves start at lower frequencies due to the larger sizes of the smallest deployed arrays (Table 1). At Aigio, the dispersion curve derived from NERIES data shows a complex shape and large standard deviations between 15 and 30 Hz. Part of this frequency range is influenced by a sharp spectral peak around 25 Hz, with large amplitudes on the vertical components, that was observed during the recording of the smallest array, but not during the following recordings of the larger arrays. In the urban environment of the site, this kind of sharp and temporally variable peak is likely caused by some machinery. In fact, it is probably due to work on the street light electrics that was performed close to the array location during the recording of the smallest array. However, the deviation of the dispersion curve to lower slownesses between 18 and 22 Hz can also be explained by the influence of a higher mode which is not generated at lower frequencies. At Colfiorito, the derived Rayleigh wave dispersion curves show an excellent agreement for both Rayleigh fundamental and higher mode. At Korinthos, a similarly good agreement is obtained over a

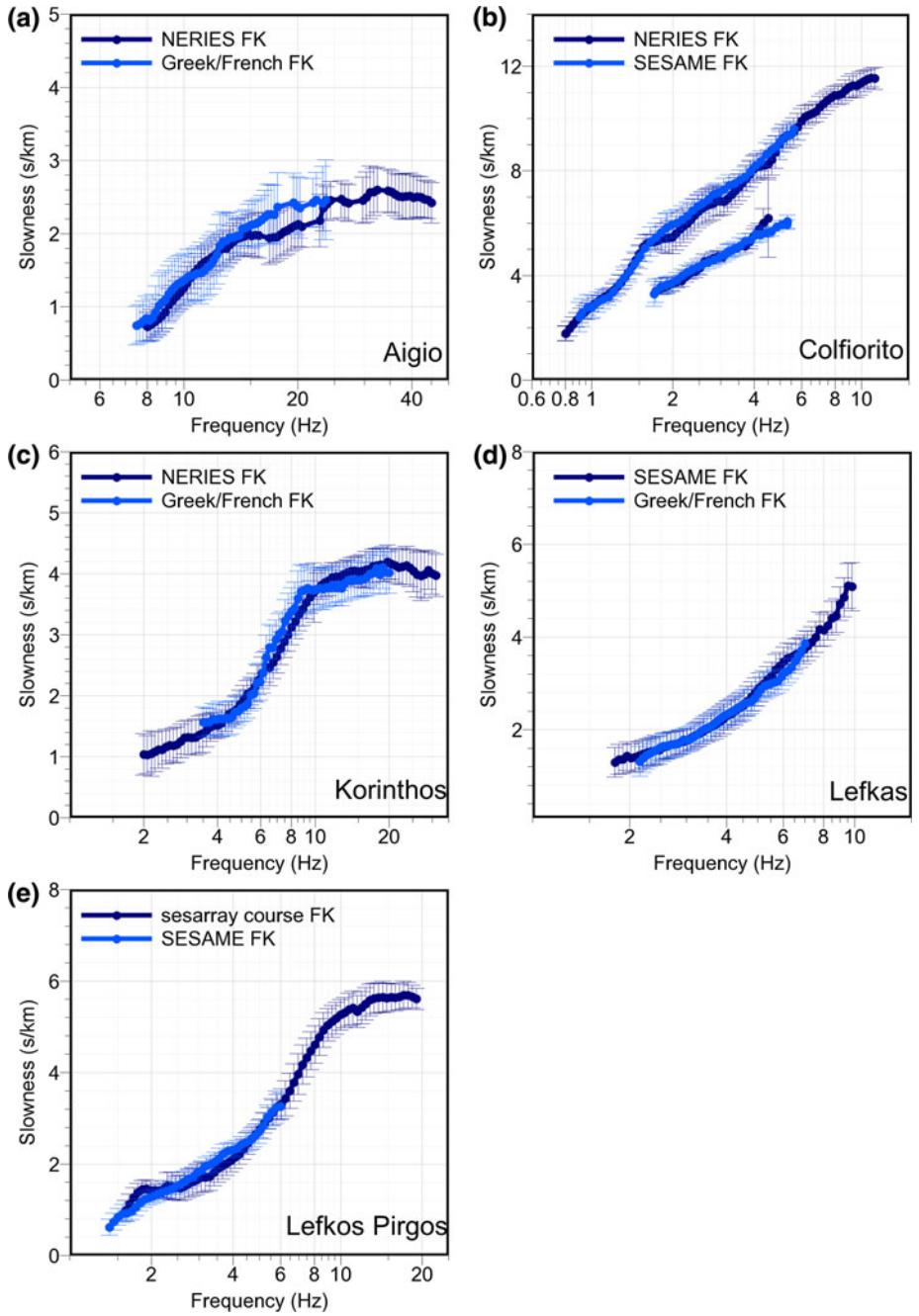

Fig. 7 Comparison of Rayleigh wave dispersion curves derived from FK for repeated ambient vibration measurements at the same location

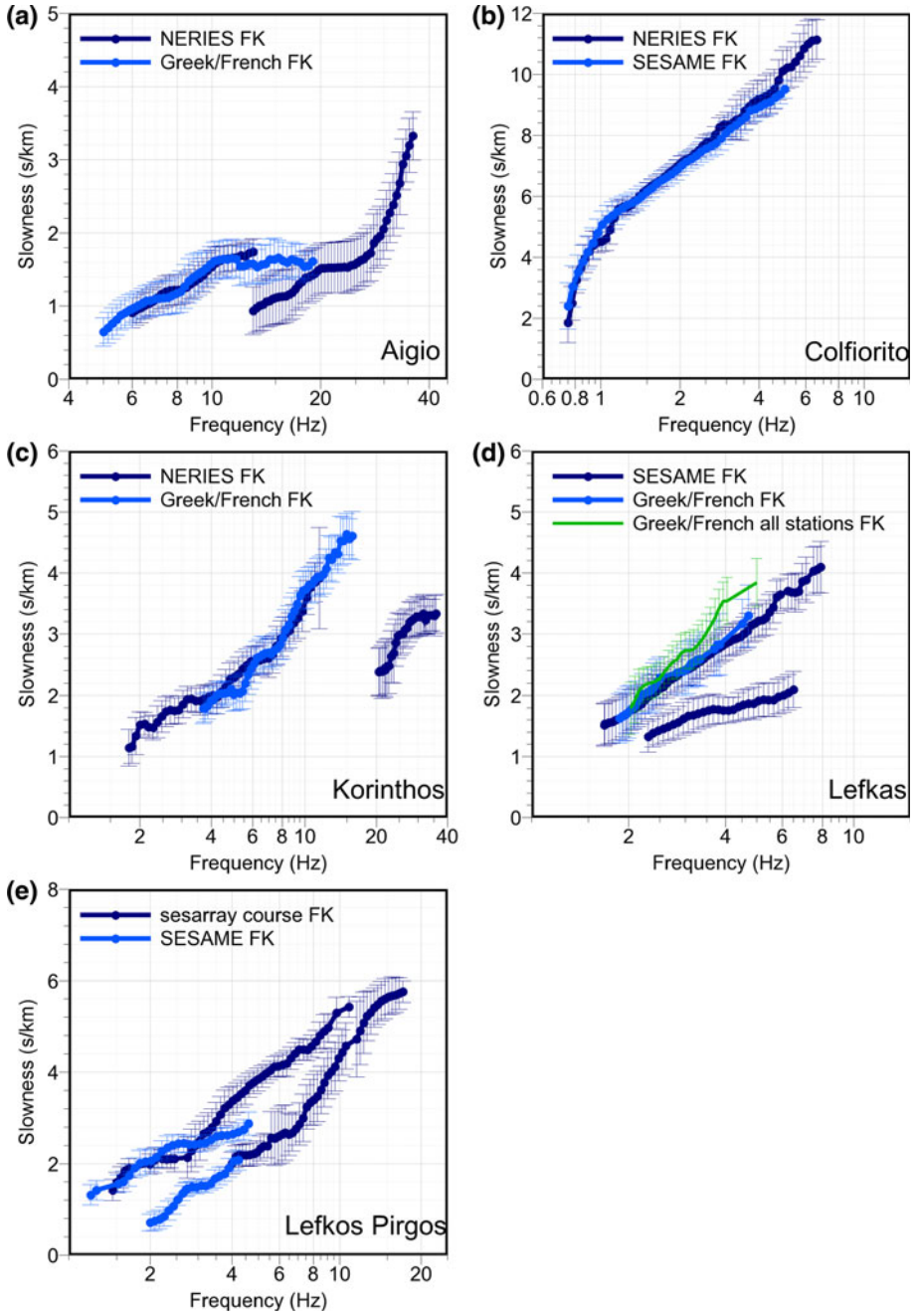

Fig. 8 Same as Fig. 7, but for Love waves. For Lefkas, *thin*, *green line* indicates original result of FK processing using all stations of the medium array, *while thicker*, *light blue line* shows the result after excluding a station with problematic horizontal components

wide frequency range, while at Lefkas and Lefkos Pirgos, the overlapping frequency range is smaller, but the agreement still fine.

For the Love wave dispersion curves derived from FK (Fig. 8), the agreement between dispersion curves from different measurement campaigns is also very good, though in some urban locations the analysis of horizontal components proved more difficult. At Aigio, Korinthos and Lefkas, a Love wave higher mode could only be detected in one of the two measurements—the one that was capable of reaching higher frequencies. For Aigio, the Love wave dispersion curve derived from the Greek/French cooperation data shows mode jumping at frequencies above 11 Hz—it deviates from the fundamental mode dispersion curve and approaches the higher mode dispersion curve as derived from NERIES data. With only the Greek/French dataset available, it would become very difficult to correctly identify this tendency. For the rural location at Colfiorito, the agreement between curves is once more excellent, and very good correspondence is also observed for the urban site of Korinthos.

For Lefkas, and, more pronounced, for Lefkos Pirgos, there is a discrepancy between the measured Love wave dispersion curves at high frequencies. At Lefkas, both curves are still, though barely, contained within each other's standard deviation, which is no longer the case for Lefkos Pirgos. As these are the two sites with the most urban environment of all locations considered, where stations were installed directly next to roads, the observed discrepancies might point to general problems with the interpretation of horizontal components in a difficult measurement environment with heavy and local cultural noise.

Indeed, at Lefkas it was not possible to obtain any dispersion curve from the horizontal components of the smallest array of the Greek/French deployment. For the smallest two arrays, the spectra of both horizontal components of the central station show a strong rise in amplitudes for frequencies below 3 Hz and exceptionally large amplitudes in this frequency band, up to eight times as large as the average of the other stations. Still, analysis without the central station does not improve the FK results for the smallest array as the concerned frequency range is below the resolution limit of this array. For the medium array, another station, the one due East of the centre, also shows anomalous spectra, with a peak twice the amplitude of the other stations around 4 Hz on both horizontal components. This observation can be explained by horizontal motion or tilting of the seismometer due to a close-by, strong noise source (e.g. traffic or people passing immediately next to this individual seismometer). It might have a strong influence on the part of the dispersion curve estimated from the data of this array (Forbriger 2009), i.e. the higher-frequency part of the dispersion curve that shows the discrepancy to the SESAME measurement. FK analysis without this problematic station indeed leads to a curve that can be followed to higher frequencies and is much closer to the SESAME data. Compensating for this kind of problems occuring on a single station's horizontal components during in-town measurements is probably easier if the array deployment contains a larger number of stations than was available during the Greek/French campaign. With only 6 stations, the influence of each individual station is larger and it becomes more important that each station is working correctly.

At Lefkos Pirgos, several explanations are possible for the observed high-frequency differences. On the one hand, similarly to the measurements at Aigio, the fundamental mode curve derived from SESAME data might actually lie between the fundamental and higher mode above 3 Hz. It approaches the observed higher mode curves, while the fundamental and higher mode curves derived from the sesarray experiment are more or less parallel at these frequencies. On the other hand, another possible reason for the discrepancies between the two measurements are actual lateral structural variations. At this location, the centres of the arrays used in both experiments are more than 300 m apart, the largest distance of all locations considered for the repeated measurements (Fig. 2). The smallest interstation distances close

to the array centres are used in the dispersion estimation at the highest frequencies. At 5 Hz, the highest frequency covered by both curves simultaneously, the wavelength is estimated to be around 65 m from the measured phase velocities, indicating that the arrays were separated by several wavelengths at this frequency. Thus, the two experiments might easily sample different structures at depth within the heavily reworked and urbanized environment at Lefkos Pirgos. As the sensitivity of Love waves is more concentrated in the shallowest part of the underground than the one of Rayleigh waves of the same frequency, this effect is expected to be more pronounced for Love waves. Besides, higher modes at the same frequency are influenced by structure at larger depth than the fundamental mode, which can explain the observed good agreement between the two measurements for the Love wave higher mode dispersion curves. In addition, some general shallow structural variation due to the different seasons during which the measurements were conducted (high summer vs. early winter) can neither be completely excluded.

4.4 Spatial autocorrelation curves

The three components of the spatial autocorrelation functions from the repeated measurements at the five locations are shown in Fig. 9. For each site, the curves are shown for three to five logarithmically equidistant frequencies between the upper and lower limit for which both Love and Rayleigh wave dispersion curves could reliably be derived from the autocorrelation functions. Theoretically calculated values for the Bessel function expressions describing each of the components are shown together with the measured data to give an additional impression of the goodness of fit. They are calculated using the phase velocities and average values of α derived from the joint grid-search inversion of all three-component MSPAC data at the corresponding frequencies (Köhler et al. 2007), which results in Rayleigh and Love wave dispersion curves and values for α as illustrated for Volvi in Fig. 6. For all sites, a generally very good agreement between the spatial autocorrelation values from different arrays belonging to one experiment as well as between the two repeated measurements is observed, in some cases to quite low frequencies (e.g. 0.8 Hz in the case of Colfiorito) and in others up to several zero-crossings of the autocorrelation function (e.g. Korinthos). Often, the measured points follow a common curve not only for the vertical, but also for the radial and transverse components, which indicates that there is no large variation in the relative amount of Love and Rayleigh wave energy between the individual measurements. For example, for a frequency of 1.25 Hz the data on the radial and transverse components at Colfiorito (Fig. 9b) clearly show a much better agreement with the theoretical curve for α equal to 0.15 (dashed line) than to the curve for a larger value of 0.5 for α (solid line), indicating a larger Love wave contribution to the wave field. Both theoretical curves are drawn, however, as the α values determined from the NERIES data show large variations around 1.25 Hz. There are some exceptions, i.e. the radial and transverse SPAC curves at the lowest frequencies in Aigio and Korinthos. In these cases, a different value of α is required to fit both of the measurements equally well.

The observed deviations from the theoretical curves also show some common characteristics: They mainly occur for the smallest ring radii and at low frequencies (Aigio, Colfiorito, Lefkas and Lefkos Pirgos). This can be explained by the long wavelengths of these data compared to the ring radii that impede a meaningful correlation between the recordings of different sensors. Generally, only higher frequencies would be considered at these small ring radii to, for example, determine dispersion curves from SPAC measurements. For the comparison between different measurements, though, all rings were sampled at the same frequencies when calculating the autocorrelation curves. During the Greek/French experiment at Aigio, the smallest two arrays were measured two times, one time immediately after

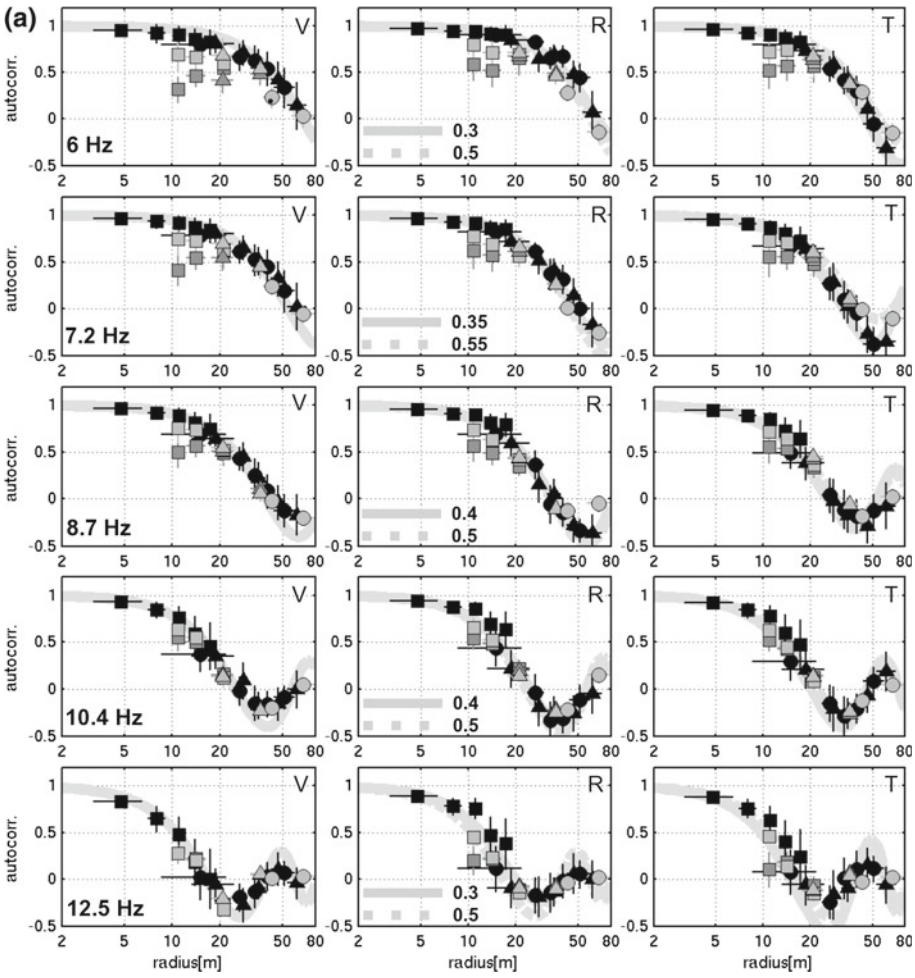

Fig. 9 (**a**) Comparison of spatial autocorrelation curves for repeated measurements at Aigio. V, R, T refer to the vertical, radial and transverse components, respectively. *Rows* from *top* to *bottom* show data at different frequencies as indicated in the plots for the vertical component. *Black* symbols with standard deviations indicate data derived from the NERIES measurements, while *gray* symbols with standard deviations show data from measurements of the Greek/French cooperation. *Different shades* of *gray* are from two consecutive measurements with the same arrays. *Different symbols* refer to measurements from different arrays, with increasing array diameters depicted by *squares*, *triangles* and *circles*, respectively. *Light gray curves* represent theoretically calculated spatial autocorrelation functions for the respective frequencies, the Rayleigh and Love wave velocities and the Rayleigh-to-Love ratio α inferred from the measurements by joint grid-search inversion of all three components of all SPAC curves. *Solid and dashed light gray curves* for the radial and transverse components refer to the different values of α found for the repeated measurements, as stated in the legend in the plot of the radial curves for each frequency **b** same as **a** for Colfiorito. *Black symbols* refer to NERIES measurements, while *gray symbols* depict SESAME measurements **c** same as **a** for Korinthos at. *Black symbols* indicate NERIES data (data points from fourth and largest array depicted by *diamonds*), while *gray symbols* refer to the Greek/French cooperation project **d** same as **a** for Lefkas. *Black symbols* indicate SESAME measurements while *gray symbols* show data from the Greek/French cooperation **e** same as **a** for Lefkos Pirgos (Thessaloniki). *Black symbols* indicate SESAME data, while data from the sesarray course are plotted in *gray*

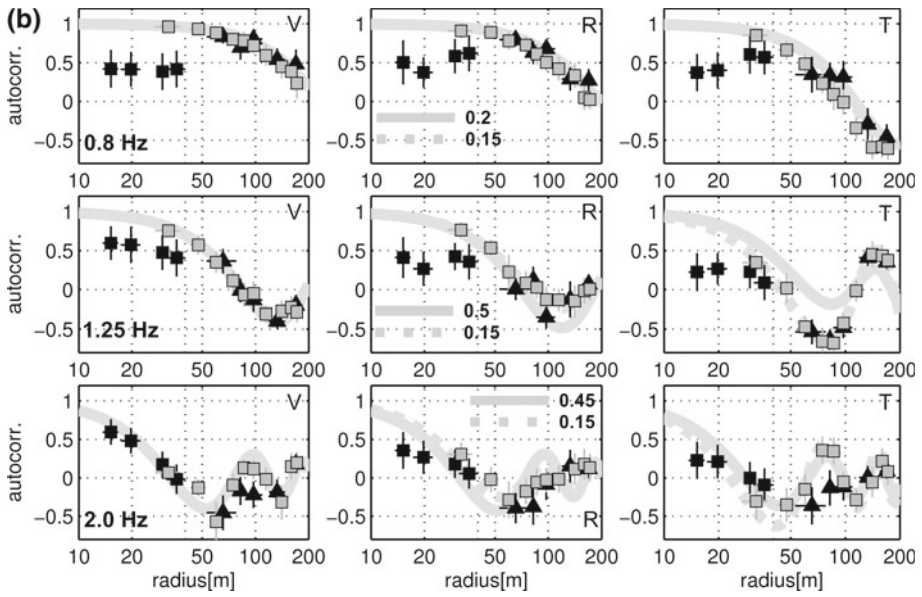

Fig. 9 continued

the other, as seismograms of the first measurement looked rather noisy and unsatisfactory. This can be confirmed by looking at the autocorrelation curves which show a larger deviation from the expected values for the first set of measurements. At Korinthos, a single outlier from the measurements is observed for a ring radius of 13.34 m, which is the largest ring of the smallest array from the Greek/French experiment, at high frequencies (6.3 Hz and 8.5 Hz).

Interestingly, the differences observed in the Love wave dispersion curves derived by FK for Lefkas are not apparent in the transverse component of the SPAC curves. At frequencies above 3 Hz, where the deviation in the dispersion curves is evident, the SPAC data from both measurements still agree closely with the same Bessel-type curve (Fig. 9d). This might be an indication that SPAC analysis is more tolerant of the type of problem affecting the horizontal components in this urban location.

5 Discussion

The analysis of the average spectral and propagation properties of the ambient vibration array measurements shows that the noise wavefield is variable with time, for example due to different anthropogenic activity or different meteorological conditions. However, in all cases this variability, which has previously been observed in other measurements (e.g. Panou et al. 2005; Bonnefoy-Claudet et al. 2006a; Vassalo et al. 2008), shows little influence on the dispersion curves derived by FK and on the SPAC curves extracted from the array recordings. For urban as well as rural sites and for shallow (i.e. Aigio, Lefkas) as well as large (i.e. Volvi, Lefkos Pirgos) bedrock depths (Table 2), the dispersion and SPAC curves show good agreement between different measurements. For all sites, the dispersion curves from both measurements are contained within each other's standard deviation, which means that they can be explained by compatible sub-surface structure. The curves are also consistent

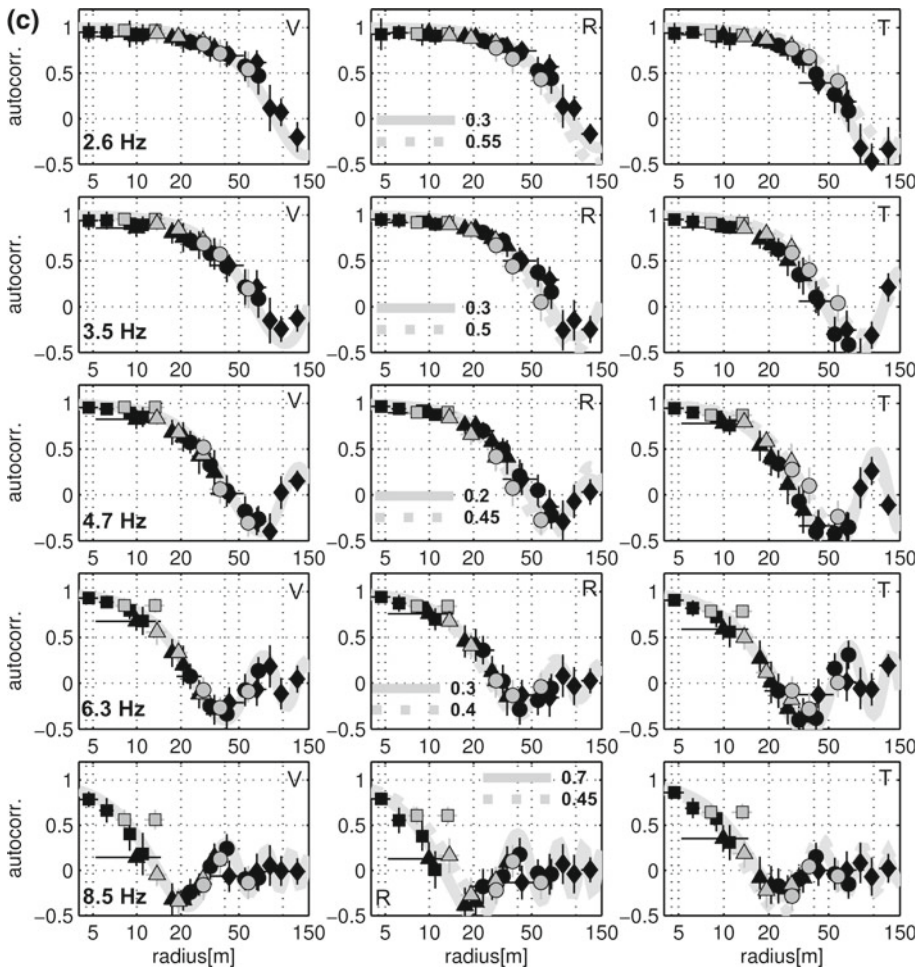

Fig. 9 continued

between different arrays from a single installation, and the dispersion curves derived from SPAC agree very well with the results of the FK. In addition, for the NERIES sites dispersion curves from active seismic measurements (Multichannel Analysis of Surface Waves, MASW) that were conducted simultaneously with the array recordings, were available for comparison (Endrun and Renalier 2008). In general, the MASW dispersion curves cover a slightly different frequency range than the ambient vibration array data, extending to higher frequencies (up to 50–60 Hz), but missing the low-frequency part of the dispersion curve (below 5–10 Hz), though details depend on the configuration of the respective measurements. However, in the frequency range covered by both active and passive measurements, the agreement is good for all sites considered here (Aigio, Colfiorito, Korinthos and Volvi) for Love as well as Rayleigh waves.

The excitation and visibility of higher modes within the ambient vibration wavefield might vary from one measurement and one set of measurement conditions to the other, especially for Love waves (for example, see dispersion curves for Aigio, Korinthos and Lefkas). The

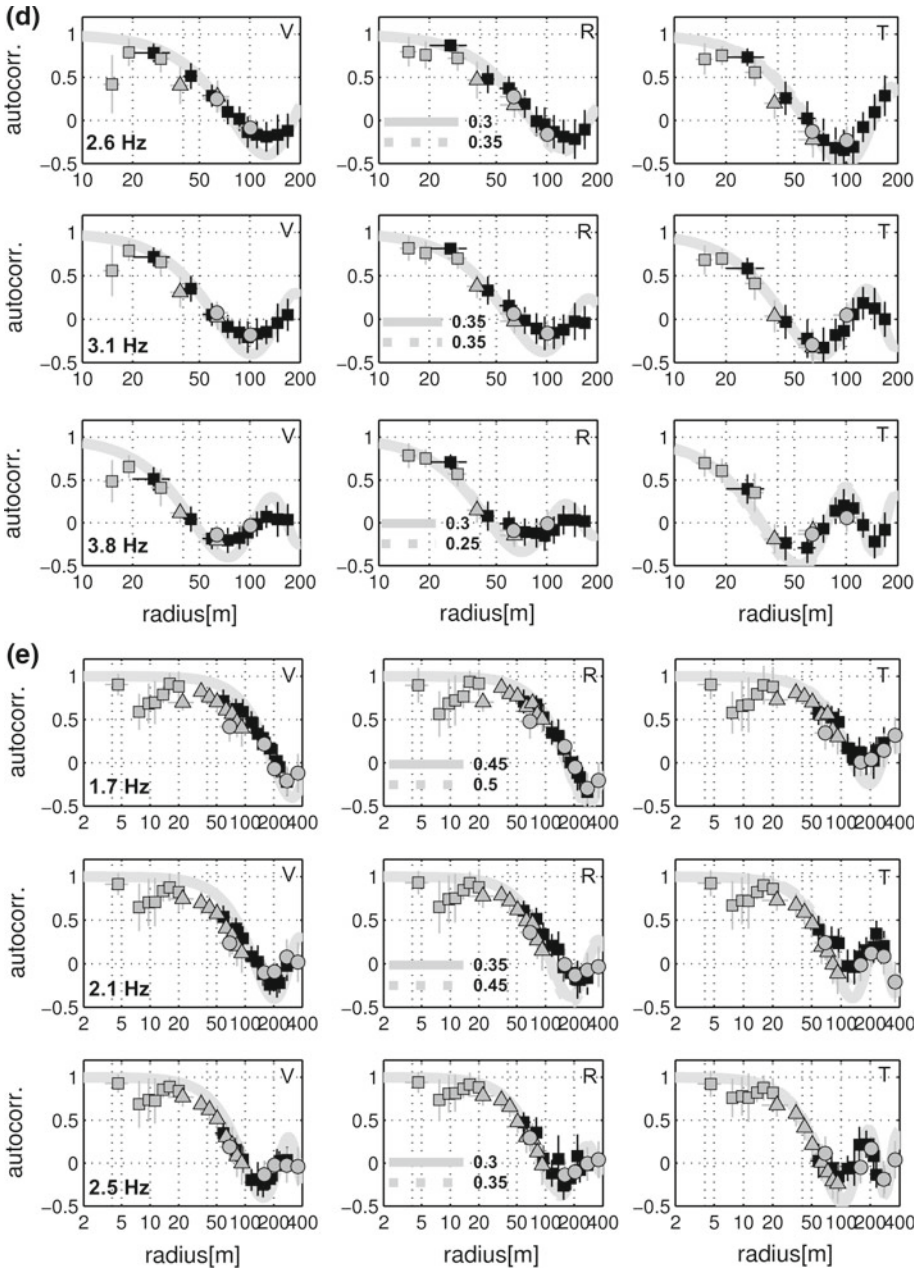

Fig. 9 continued

SESAME measurements at Colfiorito, which lasted for 15 h, lead to an interesting observation in this context: The Rayleigh wave higher mode, which is clearly observed during the early hours of the morning (from 04:00 am to 09:00 am) in the FK data from this array, cannot be found during the middle of the night (11:00 pm to 04:00 am). It seems that the clear excitation of the higher mode is dependent on the source distribution: The energy distribution

between fundamental mode and higher modes in the ambient-vibration wavefield is known to dependent on the distance distribution of the sources, as damping leads to a preferential attenuation of the fundamental mode for more distant sources (SESAME 2005). Accordingly, the observation of the higher mode during certain time windows or during one of two repeated measurements indicates that either a strong, distant source capable of mainly exciting the higher mode was only active during this time windows or strong, close sources that transmit energy mainly to the fundamental mode were inactive during this time windows, permitting the higher mode to be seen. The temporal variability of long-term array measurements will be the subject of further study.

Accordingly, while it is hard to find indications of variations in the frequency band that is covered by the dispersion curve due to the activity or inactivity of distinct sources in the comparison of the repeated measurements—mainly due to the variations in array layout that have similar and competing effects—the variable visibility of higher modes hints at this kind of fluctuations in the noise wavefield. The additional information given by a higher mode dispersion curve—if correctly identified—can help during inversion to further constrain the velocity profiles that might explain the data. However, while some models might be excluded based on the additional information, no fundamentally different type of velocity models is expected.

It is remarkable that higher modes are observed during at least one of the two repeated measurements at five of the six sites for Love waves, but only at one site, Colfiorito, for Rayleigh waves. This observation agrees with what is predicted, for example, by Fäh et al. (2008), who state that one of the advantages in using horizontal component data is that the separation between different modes is larger for Love waves, and thus, they are easier to identify. Intriguingly, the only site where a Rayleigh wave higher mode is observed is the only one where no Love wave higher mode is found, even though the Love wave contribution to the wavefield is very large for this site. This, together with the variable observance of the Love wave higher mode between repeated measurements (e.g. at Aigio, Korinthos and Lefkas) and, most strikingly, the temporally variable occurrence of the Rayleigh higher mode during the continuous measurements at Colfiorito, illustrates the importance of appropriate sources generating energy in the right frequency-wavenumber band for the observability of higher modes in the ambient vibration wavefield.

While the dispersion and SPAC curves do not vary between repeated measurements, the relative amount of Rayleigh wave energy in the wavefield can change, probably due to the activity of different sources. Variations are for example found for the two lowest frequencies (6 and 7.2 Hz) at Aigio (Fig. 9a), where the fit of measured data with the theoretical Bessel-function type curves for the largest array radii on the horizontal components points to a different and larger value of α during the Greek/French experiment (around 0.5) compared to the NERIES measurements (around 0.3). A similar observation can be made for the lowest frequencies (2.6, 3.5 and 4.7 Hz, respectively) at Korinthos (Fig. 9c), where again a larger value of α (around 0.5 vs. 0.3) is found during the Greek/French experiment. At higher frequencies (8.5 Hz) the measured data at small radii point to an exceptionally large value of α for the NERIES measurement (around 0.7), while the Greek/French experiment still shows a consistent value of around 0.5. Contrastingly, for the sites at Lefkas (Fig. 9d) and Lefkos Pirgos (Fig. 9e), which are similarly located in an urban environment, the relative contribution of Rayleigh waves is consistent between the repeated measurements at all frequencies, even though different sources contribute to the wavefield (Fig. 5). The same holds true for the rural site of Colfiorito, where a very low amount of Rayleigh waves (α about 0.15) is observed at all frequencies (Fig. 9b). This tendency towards lower values of α is also found in the data from Volvi, which are not displayed here. In general, Fig. 9 shows that the value of α

is at or below 0.5 at all frequencies for all measurements, indicating a strong contribution of Love waves to the ambient vibration wavefield. Additionally, α is not constant, but variable with frequency and seems to be especially low for the rural sites. Similar observations of at least 50% and up to 90% Love waves in the ambient vibration wavefield have been reported for single sites (e.g. Köhler et al. 2007; Bonnefoy-Claudet et al. 2008), but the results from SPAC shown here indicate this to be a common case in a wide variety of settings, even if the individual sources of the wavefield vary.

The different array configurations, using between 6 and 13 stations in a single array, do not have any discernible influence on the resulting dispersion curves, apart from the fact that the minimum and maximum aperture of the deployed arrays (Table 1) influences the frequency range across which the dispersion curves can be determined. For example, in the case of Korinthos, the smallest array radius in the case of the NERIES measurements was 5 m, while the largest one is ∼60 m. The Rayleigh wave dispersion curve was determined between 30 and 2 Hz from these data. In the Greek/French experiment, the smallest array radius was 8 m and the largest 30 m, and the Rayleigh wave dispersion curve could only be determined between 20 and 3.5 Hz. The precise frequency range that can be covered by a given array size depends on the local velocity structure and also on the frequency and distance distribution of noise sources. Besides, with a larger number of stations available, less individual arrays have to be deployed to cover the same frequency range. For example, compare the Rayleigh wave dispersion curve derived from three six-station arrays of increasing size in the Greek/French experiment and the curve derived from a single 13-station array deployed during SESAME in Lefkas. In this case, it is possible to extend the dispersion curve to high as well as low frequencies arrays using a single array, which contains smaller and larger interstation distances than the three arrays deployed during the Greek/French experiment (Table 1).

The instrumentation used neither seems to influence the resulting data products significantly. Most of the measurements actually used the same seismometer, Lennartz's 5 s, which was found to be the overall best sensor of those tested for measurements down to 0.1 Hz by Guillier et al. (2008). Their comparative test of digitizers, sensors and digitizer-sensor couples was aimed at deriving recommendations for ambient vibration H/V measurements. However, the tests of the consistency, accuracy and stability of the different instruments have general applicability, also for stations used in another context. The study of Guillier et al. (2008) did not include the Guralp CMG6-T instrument, which was not available at the time the study was conducted (SESAME 2002b). A Guralp 30 s seismometer, though, was used in the test, and showed very good results in terms of signal shape in time and spectral domains. All of the digitizers—again except the built-in one in the CMG6-T—used during the repeated measurement were investigated by Guillier et al. (2008). They observe good consistency between channels, no drift or polarity problems and a sensitivity close to the one specified by the manufacturer for all three digitizer types. This is consistent with our observation that no clear influence of the used equipment on the resulting data products can be determined. Rather, the measured dispersion and SPAC curves are independent of the equipment used—as far as tested in this study, e.g. we cannot confirm the satisfactory performance of 4.5 Hz sensors as observed by Guillier et al. 2008. Likewise, we cannot derive any recommendations on the necessary measurement durations for ambient vibration recordings—from the consistency of results, it seems that each of the recordings lasted long enough to provide a stable estimate of the dispersion and SPAC curves.

Comparing the results for the sites where the seasonal conditions between the two measurements differ most, i.e. Colfiorito (early spring, with snow still covering the mountains around the valley, vs. high summer) and Lefkos Pirgos (high summer, with large heat during the day, vs. winter), no systematic variations are apparent. Precipitation data (ECMWF

ERA-interim dataset) shows that no heavy rains occurred at either of the two locations in the week before either of the repeated measurements. However, the volumetric soil moisture (determined for the uppermost 2.89 m of the subsurface) shows some variations with season for both locations (ECMWF ERA-interim dataset). At Lefkos Pirgos, variability in soil moisture is large (around 25%) only for the uppermost soil layers (to 21 cm depth) and decreases rapidly below, to average around 5% for the total depth range to 2.89 m. This is clearly insufficient to explain the observed Love wave fundamental mode discrepancies at high frequencies. Rather, they can be convincingly explained by the influence of higher modes or the sampling of different structures (see Sect. 4.3). At Colfiorito, the differences in soil moisture content are larger, showing an average increase by 20% across the 2.89 m depth range during the NERIES measurement in early spring compared to the SESAME acquisition in summer. Velocity variations in such shallow depths, however, cannot be resolved by our measurements, which in this case are only influenced by velocity changes below ~2.5 m depth for the NERIES Rayleigh wave dispersion curve and below ~6 m depth for the SESAME data. Though the soil moisture may vary to larger depths than covered by the soil moisture model, at least the values provided by the model are hardly—if at all—covered by the datasets, preventing a meaningful comparison of the influence of different volumetric soil moisture contents. The measured Love and Rayleigh wave dispersion curves at Colfiorito actually show excellent agreement, indicating that any possible seasonal variation of sub-surface properties is below the resolution threshold of the ambient vibration array measurements. With the use of smaller arrays (e.g. starting with 5 m diameter like for the NERIES measurements in Aigio and Korinthos), this could potentially change, if dispersion curves could be determined to higher frequencies, especially at slow sites like Colfiorito, Volvi and Lefkas. With the present dataset, though, further investigation of this question is not possible.

Another seasonal effect that is related to changes in the noise wavefield rather than variations in the subsurface conditions can be observed in the data: The variability in the excitation of microseisms (Fig. 4b). However, the corresponding frequency is so low that it can hardly be resolved in FK analysis even by the largest arrays used in this study. Tanimoto et al. (2006) and Tanimoto and Alvizuri (2006) report an influence of the seasonal source location changes of long-period microseisms on the long-period (0.1–0.2 Hz) H/V ratio, explained by variable contributions of higher modes. The possible impact of this seasonal variability on long-period ambient vibration dispersion measurements would also warrant further investigation, using larger and non-temporary arrays, though.

Some variations in the noise wavefield with the day of week are found in the measurements, e.g. in Fig. 4b) which compares spectra measured at Volvi on a weekday (SESAME) to those measured at the weekend (NERIES). A similarly enhanced noise level between 2 and 4 Hz is also observed when comparing the SESAME measurement (performed on Monday and Tuesday) with the NERIES measurement (conducted on a Sunday) at Colfiorito. Here, the noise amplitude doubles for the weekday compared to the weekend. However, as these two rural sites provide very good agreement between dispersion curves for the repeated measurements (Figs. 6, 7, 8), no adverse effects of the varying noise generation can be found. Due to the limitations of the dataset, a further systematic comparison between noise recordings at different times of day is not possible and may be subject of future projects.

In general, we observe excellent agreement between dispersion and SPAC curves measured during different years at different times of day on different weekdays in different seasons by different teams using different array layouts and different instrumentation. This indicates that, though the noise wavefield is variable at high as well as at low frequencies on the time scales considered here, the measurement results are independent of these variations and repeatable. Accordingly, variations of up to 50% in slowness as well as velocity observed in the sub-

surface models resulting from a recent blind test (Cornou et al. 2009) cannot be ascribed to different measurement conditions or problems in the determination of the dispersion curve, but are very likely due to uncertainties and differences in the applied inversion schemes. This can already partly be inferred from the experiment of Cornou et al. (2009), where, in addition to real data, synthetic datasets were used, thus excluding effects of the field measurements, and only inversion results that were not based on any gross misestimation of phase velocity or misidentification of modes are presented. However, it implies that future work aimed at improving the usefulness of ambient vibration recordings for site characterisation should mainly be focused on the inversion issue, for example allowing a better comparison of results by also producing reasonable uncertainty estimates for the depth profiles.

6 Conclusions

In summary, our study shows that while average properties of the ambient vibration wavefield, i.e. strength, number and location of sources, vary with time, the derived data products, i.e. dispersion and SPAC curves, can be reproduced in a stable and consistent fashion. They also prove to be independent of the team conducting the measurements, the instrumentation and array-layout used and the timing (within the year as well as within the week or day) and duration of the measurements, at least within the limits investigated here. The frequency range over which the dispersion and SPAC information can be determined and used primarily depends on the array layout—with a large number of station (more than 10), a single array containing both large and small interstation distances can be sufficient to cover the whole frequency-range of interest. However, if less stations are available, it is necessary to deploy several arrays of different sizes to achieve similar coverage in the frequency-wavenumber space. The observability of higher modes, which depends on the underground structure as well as on the sources contributing to the wavefield, is variable and hard to predict in advance. Based on the data from the six sites examined here, the stability and consistency of the ambient vibration data products is best for rural sites without much anthropogenic noise sources located close to or even inside the arrays. However, good agreement is also found for urban locations, especially for Rayleigh waves, while the analysis of horizontal components, specifically in urban locations, requires careful data analysis procedures and critical interpretation. To sum up, array recordings of ambient vibrations do indeed contain structural information and can be used to gather information on the shallow subsurface structure in a relatively quick, cost-efficient and nondestructive way. The main reason for the variability observed in inversion results from recent blind tests using ambient vibration datasets is thus probably unrelated to problems in the field measurements or the determination of dispersion and SPAC curves from the data.

Acknowledgments This work was funded by the EC-project NERIES, JRA4. The EC Marie Curie exchange program provided funding for research visits of A. Savvaidis to Potsdam. Data from the Greek/French experiment were courteously provided by ITSAK, Thessaloniki. We would especially like to express our gratitude for aid in the planning, logistics and performance of the field-measurements to ITSAK, Thessaloniki (SESAME and NERIES), and NOA, Athens (NERIES), in Greece, and to INGV Roma and Napoli (SESAME) and DPC Roma (NERIES) in Italy. ECMWF ERA-interim data as provided on the ECMWF data server were used. Comments by an anonymous reviewer and a thorough review by M. Asten helped to improve this paper and are gratefully acknowledged.

References

Aki K (1957) Space and time spectra of stationary stochastic waves, with special reference to microtremors. Bull Earthq Res Inst Tokyo Univ 25:415–457

Anastasiadis A, Raptakis D, Pitilakis K (2001) Thessaloniki's detailed microzoning: subsurface structure as basis for site response analysis. Pure Appl Geophys 158:2597–2633

Asten MW (2006) On bias and noise in passive seismic data from finite circular array data processed using SPAC methods. Geophysics 71(6):V153–V162. doi:10.1190/1.2345054

Asten MW (2009) Site shear velocity profiles interpretation from microtremor array data by direct fitting of SPAC curves. In: Bard P-Y, Chaljub E, Cornou C, Cotton F, Gueguen P (eds) 3rd International symposium on the effects of surface geology on seismic motion, vol. 2. Grenoble, France, 30 August–1 September 2006, Laboratoire Central des Ponts et Chaussées, pp 1069–1080 (in press)

Asten MW, Dhu T, Lam N (2004) Optimised array design for microtremor array studies applied to site classification; comparison of results with SCPT logs. 13th WCEE. Vancouver, B.C., Canada. 1–6 August 2004. Paper No. 2903

Asten MW, Boore DM (2005) Comparison of shear-velocity profiles of unconsolidated sediments near the Coyote borehole (CCOC) measured with fourteen invasive and non-invasive methods. In: Asten MW, Boore DM (eds) Blind comparison of shear-wave velocities at closely spaced sites in San Jose, California. USGS Open-File Report 2005-1169. Available at http://pubs.usgs.gov/of/2005/1169. Accessed 25 Aug 2009

Aster RC, McNamara DE, Bromiski PD (2008) Multi-decadal climate-induced variability in microseisms. Seismol Res Lett 79:194–202

Athanasopoulos GA, Pelekis PC, Leonidou EA (1999) Effects of surface topography on seismic ground response in the Egion (Greece) 15 June 1995 earthquake. Soil Dyn Earthq Eng 18(2):135–149

Beilecke T, Bram K, Buske S, Krawczyk C (2008) Influence of near surface ground conditions on seismic monitoring setups. Geophys Res Abs Vol 10(EGU General Assembly 2008):EGU2008–A09554

Bensen GD, Ritzwoller MH, Barmin MP, Levshin AL, Lin F, Moschetti MP, Shapiro NM, Yang Y (2007) Processing seismic ambient noise data to obtain reliable broad-band surface wave dispersion measurements. Geophys J Int 169:1239–1260. doi:10.1111/j.1365-246.X.2007.03374.x

Bonnefoy-Claudet S, Cotton F, Bard P-Y (2006a) The nature of noise wavefield and its applications for site effect studies—a literature review. Earth-Sci Rev 79:205–227. doi:10.1016/j.earscirev.2006.07.004

Bonnefoy-Claudet S, Cornou C, Bard P-Y, Cotton F, Moczo P, Kristek J, Fäh D (2006b) H/V ratio: a tool for site effect evaluation. Results from 1-D noise simulations. Geophys J Int 167:827–837. doi:10.1111/j.1365-246.X.2006.03154.x

Bonnefoy-Claudet S, Köhler A, Cornou C, Wathelet M, Bard P-Y (2008) Effects of Love waves on microtremor H/V ratio. Bull Seism Soc Am 98(1):288–300. doi:10.1785/0120070063

Boore DM, Asten MW (2008) Comparision of shear-wave slowness in the Santa Clara Valley, California, using blind interpretation of data from invasive and noninvasive methods. Bull Seism Soc Am 98(4):1983–2003. doi:10.1785/0120070277

Bettig B, Bard P-Y, Scherbaum F, Riepl J, Cotton F, Cornou C, Hatzfeld D (2001) Analysis of dense array noise measurements using the modified spatial auto-correlation method (SPAC): application to the Grenoble area. Boll Geofis Teo Appl 42:281–304

Burtin A, Bollinger L, Vergne J, Cattin R, Nábělek JL (2008) Spectral analysis of seismic noise induced by rivers: a new tool to monitor spatiotemporal changes in stream hydrodynamics. J Geophys Res 113:B05301. doi:10.1029/2007JB005034

Capon J (1969) High-resolution frequency-wavenumber spectrum analysis. Proc IEEE 57(8):1408–1418

Capon J (1972) Long-period signal processing results for LASA, NORSAR, and ALPA. Geophy J Roy astr Soc 31:279–296

Cara F, Di Giulio G, Rovelli A (2003) A study on seismic noise variations at Colfiorito, Central Italy: implications for the use of H/V spectral ratios. Geophys Res Lett 30(18):1972. doi:10.1029/2003GL017807

Cessaro RK (1994) Sources of primary and secondary microseisms. Bull Seism Soc Am 84(1):142–148

Chávez-García FJ, Raptakis D, Makra K, Pitilakis K (2000) Site effects at euroseistest—II. Results from 2D numerical modeling and comparison with observations. Soil Dyn Earthq Eng 19:23–39

Chávez-García FJ, Rodríguez M, Stephenson WR (2005) An alternative approach to the SPAC analysis of microtremors: exploiting stationarity of noise. Bull Seism Soc Am 95(1):277–293. doi:10.1785/0120030179

Chávez-García FJ, Rodríguez M, Stephenson WR (2006) Subsoil structure using SPAC measurements along a line. Bull Seism Soc Am 96(2):729–736. doi:10.1785/0120050141

Cho I, Tada T, Shinozaki Y (2004) A new method to determine phase velocities of Rayleigh waves from microseisms. Geophysics 69(6):1535–1551. doi:10.1190/1.1836827

Cho I, Tada T, Shinozaki Y (2006a) Centerless circular array method: inferring phase velocities of Rayleigh waves in broad wavelength ranges using microtremor records. J Geophys Res 111:B09315. doi:10.1029/2005JB004235

Cho I, Tada T, Shinozaki Y (2006b) A generic formulation for microtremor exploration methods using three-component records from a circular array. Geophys J Int 165:236–258. doi:10.1111/j.1365-246X.2006.02880.x

Claprood M, Asten MW (2009) Initial results from SPAC, FK and HVSR microtremor surveys for site hazard study at Launceston, Tasmania. Expl Geophys 40:132–142. doi:10.1071/EG08106

Cornou C, Ohrnberger M, Boore DM, Kudo K, Bard P-Y (2009) Derivation of structural models from ambient vibration array recordings: results from an international blind test. In: Bard P-Y, Chaljub E, Cornou C, Cotton F, Gueguen P (eds) 3rd International symposium on the effects of surface geology on seismic motion, vol. 2. Grenoble, France, 30 August–1 September 2006, Laboratoire Central des Ponts et Chaussées, pp 1127–1219 (in press)

De Angelis S (2008) Broadband seismic noise analysis of the Soufrière Hills volcano network. Seism Res Lett 79(4):504–509. doi:10.1785/gssrl.79.4.504

De Becker M (1990) Continuous monitoring and analysis of microseisms in Belgium to forecast storm surges along the North Sea coast. Phys Earth Planet Int 63:219–228

Di Giulio G, Rovelli A, Cara F, Azzara RM, Marra F, Basili R, Caserta A (2003) Long-duration asynchronous ground motions in the Colfiorito plain, central Italy, observed on a two-dimensional dense array. J Geophys Res 118(B10):2486. doi:10.1029/2002JB002367

Di Giulio G, Cornou C, Ohrnberger M, Wathelet M, Rovelli A (2006) Deriving wavefield characteristics and shear-velocity profiles from two-dimensional small-aperture arrays analysis of ambient vibrations in a small-size alluvial basin Colfiorito, Italy. Bull Seism Soc Am 96(5):1915–1933. doi:10.1785/0120060119

Doutsos T, Poulimenos G (1992) Geometry and kinematics of the active faults and their seismotectonic significance in the western Corinth-Patras rift (Greece). J Struct Geol 14(6):689–699

Drouet S, Triantafyllidis P, Savvaidis A, Theodulidis N (2008) Comparison of site-effects estimation methods using the Lefkas Greece 2003 earthquake aftershocks. Bull Seism Soc Am 98(5):2349–2363. doi:10.1785/0120080004

Endrun B, Meier T, Lebedev S, Bohnhoff M, Stavrakakis G, Harjes H-P (2008) S velocity structure and radial anisotropy in the Aegean region from surface wave dispersion. Geophys J Int 174:593–616. doi:10.1111/j1365-246X.2008.03802.x

Endrun B, Renalier F (2008) Report on in-situ measurements at the 20 selected sites. NERIES-Project JRA4 Task C. EU-FP6 EC project number 026130. Deliverable D2. Available via http://www.neries-eu.org/main.php/JRA4_D2_main_appendix1_appendix2.pdf?fileitem=12438634. Accessed 8 May 2009

Fäh D, Stamm G, Havenith H-B (2008) Analysis of three-component ambient vibration array measurements. Geophys J Int 172:199–213. doi:10.1111/j.1365-246.X.2007.03625.x

Forbriger T (2009) About the nonunique sensitivity of pendulum seismometers to translational, angular, and centripetal acceleration. Bull Seism Soc Am 99(2B):1343–1351. doi:10.1785/0120080150

Frank SD, Foster AE, Ferris AN, Johnson M (2009) Frequency-dependent asymmetry of seismic cross-correlation functions associated with noise directionality. Bull Seism Soc Am 99(1):462–470. doi:10.1785/0120080023

Fyen J (1990) Diurnal and seasonal variations in the microseismic noise level observed at the NORESS array. Phys Earth Planet Int 63:252–268

García-Jerez A, Luzón F, Navarro M (2008) An alternative method for calculation of Rayleigh and love wave phase velocities by using three-component records on a single circular array without a central station. Geophys J Int 173:844–858. doi:10.1111/j.1365-246.X.2008.03756.x

Gorbatikov AV, Kalnina AV, Volkov VA, Arnoso J, Vieira R, Velez E (2004) Results of analysis of the data of microseismic survey at Lanzarote Island Canary Spain. Pure Appl Geophys 161:1561–1578. doi:10.1007/s00024-004-2521-6

Gouédard P, Cornou C, Roux P (2008) Phase-velocity dispersion curves and small-scale geophysics using noise correlation slantstack technique. Geophys J Int 172:971–981. doi:10.1111/j.1365-246.X.2007.03654.x

Grevemeyer I, Herber R, Essen H-H (2000) Microseismological evidence for changing wave climate in the northeast Atlantic Ocean. Nature 408:349–352

Guillier B, Chetelain J-L, Bonnefoy-Claudet S, Haghshenas E (2007) Use of ambient noise: from spectral amplitude variability to H/V stability. J Earthq Eng 11:925–942. doi:10.1080/13632460701457249

Guillier B, Atakan K, Chatelain J-L, Havskov J, Ohrnberger M, Cara F, Duval A-M, Zacharopoulos S, Teves-Costa P, the SESAME Team (2008) Influence of instruments on the H/V spectral ratios of ambient vibrations. Bull Earthq Eng 6:3–32. doi:10.1007/s10518-007-9039-0

Gurrola H, Minster JB, Given H, Vernon F, Berger J, Aster R (1990) Analysis of high-frequency seismic noise in the western United States and eastern Kazakhstan. Bull Seism Soc Am 80(4):951–970

Hanssen P, Bussat S (2008) Pitfalls in the analysis of low frequency passive seismic data. First Break 26: 111–119

Haubrich RA, Munk WH, Snodgrass FE (1963) Comparative spectra of microseisms and swell. Bull Seism Soc Am 53(1):27–37

Jongmans D, Pitilakis K, Demanet D, Raptakis D, Riepl J, Horrent C, Tsokas G, Lontzetidis K, Bard P-Y (1998) EURO-SEISTEST: determination of the geological structure of the Volvi basin and validation of the basin response. Bull Seism Soc Am 88(2):473–487

Kassaras I, Voulgaris N, Makropoulos K (2008) Determination of site response in Lefkada town (W. Greece) by ambient vibration measurements. 31st Assembly ESC. Hersonissos, Crete, Greece. 7-12 September 2008. 198-205. Available at http://www.geophysics.geol.uow.gr/papers/ESC2008/kassaras1_ESC2008_short-paper.pdf. Accessed 28 Aug 2009

King GDP, Ouyang ZX, Papadimitriou P, Deschamps A, Gagnepain J, Houseman G, Jackson JA, Coufleris C, Virieux J (1985) The evolution of the Gulf of Corinth (Greece): an aftershock study of the 1981 earthquake. Geophys J Roy astr Soc 80:677–693

Köhler A, Ohrnberger M, Scherbaum F, Wathelet M, Cornou C (2007) Assessing the reliability of the modified three-component spatial autocorrelation technique. Geophys J Int 168:779–796. doi:10.1111/j.1365-246X.2006.03253.x

Kværna T (1990) Sources of short-term fluctuations in the seismic noise level at NORESS. Phys Earth Planet Int 63:269–276

Lacoss RT, Kelly EJ, Toksöz MN (1969) Estimation of seismic noise structure using arrays. Geophysics 34:21–38

Martinod J, Hatzfeld D, Savvaidis P, Katsambalos K (1997) Rapid N-S extension in the Mygdonian graben (Northern Greece) deduced from repeated geodetic surveys. Geophys Res Lett 24(24):3293–3296

McNamara DE, Buland RP (2004) Ambient noise levels in the continental United States. Bull Seism Soc Am 94(4):1517–1527

Morikawa H, Udagawa S (2009) A method to estimate the phase velocities of microtremors using a time-frequency analysis and its applications. Bull Seism Soc Am 99(2A):774–793. doi:10.1785/0120080100

Mucciarelli M, Gallipolli MR, Arcieri M (2003) The stability of the horizontal-to-vertical spectral ratio of triggered noise and earthquake recordings. Bull Seism Soc Am 93(3):1407–1412

Mucciarelli M, Gallipolli MR, Di Giacomo D, Di Nota F, Nino E (2005) The influence of wind on measurements of seismic noise. Geophys J Int 161:303–308. doi:10.1111/j.1365-246.X.2004.02561.x

Nakamura Y (1989) A method for dynamic characteristics estimation of subsurface using microtremor on the ground surface. Q Rept Railway Tech Res Inst 30(1):25–33

Nishimura T, Uchida N, Sato H, Masakazu O, Tanaka S, Hamaguchi H (2000) Temporal changes of the crustal structure associated with the M6.1 earthquake on September 3 1998 and the volcanic activity of Mount Iwate Japan. Geophys Res Lett 27(2):269–272

Nyst M, Thatcher W (2004) New constraints on the active tectonic deformation of the Aegean. J Geophys Res 109:B11406. doi:10.1029/2003JB002830

Ohori M, Nobata A, Wakamatsu K. (2002) A comparison of ESAC and FK methods for estimating phase velocity using arbitrarily shaped microtremor arrays. Bull Seism Soc Am 92(6):2323–2332

Ohrnberger M, Vollmer D, Scherbaum F (2006) WARAN—a mobile wireless array analysis system for in-field ambient vibration dispersion curve estimation. 1st ECEES. Geneva, Switzerland. 3–8 September 2006, p 284

Okada H (2003) The microtremor survey method. Geophysical Monograph Series 12, Society of Exploration Geophysicists

Oliver J, Page R (1963) Concurrent storms of long and ultralong period microseisms. Bull Seism Soc Am 53(1):15–26

Panou AA, Theodulidis NP, Hatzidimitriou PM, Savvaidis AS, Papazachos CB (2005) Reliability of ambient noise horizontal-to-vertical spectral ratio in urban environments: the case of Thessaloniki City (Northern Greece). Pure Appl Geophys 162:891–912. doi:10.1007/s00024-004-2647-6

Parolai S, Richwalski SM, Milkereit C, Bormann P (2004) Assessment of the stability of H/V spectral ratios from ambient noise and comparison with earthquake data in the Cologne area (Germany). Tectonophysics 390:57–73. doi:10.1016/j.tecto.2004.03.024

Parolai S, Picozzi M, Richwalski SM, Milkereit C (2005) Joint inversion of phase velocity dispersion and H/V ratio curves from seismic noise recordings using a genetic algorithm, considering higher modes. Geophys Res Lett 32:L01303. doi:10.1029/2004GL021115

Peng Z, Ben-Zion Y (2006) Temporal changes of shallow seismic velocities around the Karadere-Düzce branch of the North Anatolian Fault and strong ground motion. Pure Appl Geophy 163:567–600. doi:10.1007/s00024-005-0034-6

Pham VN, Bernard P, Boyer D, Chouliaras G, Le Mouël JL, Stavrakakis GN (2000) Electrical conductivity and crustal structure beneath the central Hellenides around the Gulf of Corinth (Greece) and their relationship with seismotectonics. Geophys J Int 142:948–969

Picozzi M, Parolai S, Richwalski SM (2005) Joint inversion of H/V ratios and dispersion curves from seismic noise: estimating the S-wave velocity of bedrock. Geophys Res Lett 32:L11308. doi:10.1029/2005GL022878

Picozzi M, Sabetta F, Theodulidis N, Zacharopoulos S, Savvaidis A, Bard P-Y, Cornou C, Gueguen P, Fäh D, Kalogeras I, Akkar S, Rinaldis D, Tanircan G (2007) Selected sites and available information. NERIES-Project JRA4 Task C. EU-FP6 EC project number 026130. Deliverable D1. Available via http://www.neries-eu.org/main.php/JRA4_D1_TASK%20A.pdf?fileitem=13025315. Accessed 25 Sep 2009

Pitilakis K, Raptakis D, Lontzetidis K, Tika-Vassilikou Th, Hatzfeld D (1999) Geotechnical and geophysical description of EURO-SEISTEST using field laboratory tests and moderate strong motion recordings. J Earthq Eng 3(3):381–409

Raptakis D, Theodulidis N, Pitilakis K (1999) Data analysis of the Euroseistest strong motion array in Volvi (Greece): standard and horizontal-to-vertical spectral ratio techniques. Eq Spectra 14(1):203–224

Raptakis D, Chavez-Garcia FJ, Makra K, Pitilakis K (2000) Site effects at Euroseistest—I. Determination of the valley structure and confrontation of observations with analysis. Soil Dyn Earthq Eng 19:1–22

Raptakis D, . Manakou MV, Chavez-Garcia FJ, Makra K, Pitilakis K (2005) 3D configuration of Mygdonian basin and preliminary estimate of its site response. Soil Dyn Earthq Eng 25:871–887. doi:10.1016/j.soildyn.2005.05.005

Rigo A, Bethoux N, Masson F, Ritz J-F (2008) Seismicity rate and wave-velocity variations as consequences of rainfall: the case of the catastrophic storm of September 2002 in the Nîmes Fault region (Gard France). Geophys J Int 173:473–482. doi:10.1111/j.1365-246.X.2008.03718.x

Roberts J, Asten M (2005) Estimating the shear velocity profile of quarternary silts using microtremor array (SPAC) measurements. Expl Geoph 36:34–40. doi:10.1017/EG05034

Roberts J, Asten M (2007) Further investigation over quarternary silt using the spatial autocorrelation (SPAC) and horizontal to vertical spectral ratio (HVSR) microtremor methods. Expl Geoph 38:175–183. doi:10.1071/EG07017

Roberts J, Asten M (2008) A study of near source effects in array-based (SPAC) microtremor surveys. Geophys J Int 174:159–177. doi:10.1111/j.1365-246.X.2008.03729.x

Savvaidis AS, Pedersen LB, Tsokas GN, Dawes GJ (2000) Structure of the Mygdonia basin (NGreece) inferred from MT and gravity data. Tectonophysics 317:171–186

Savvaidis A, Cadet H, Gueguen P, Panou A, Campillo M, Theodulidis N, Kalogeras I (2006) Accelerograph stations site characterization using ambient noise: selected stations in Greece. In: Third international symposium on the effects of surface geology on seismic motion. Grenoble, France. 30 August–1 September 2006, Paper Number 064

Schevenels M, Lombaert G, Degrande G, François S. (2008) A probability assessment of resolution in the SASW test and its impact on the prediction of ground vibrations. Geophys J Int 172:262–275. doi:10.1111/j.1365-246X.2007.0326.x

Sens-Schönfelder C, Wegler U (2006) Passive image interferometry and seasonal variations of seismic velocities at Merapi Volcano Indonesia. Geophys Res Lett 33:L21302. doi:10.1029/2006GL027797

SESAME (2002a) Report on the array data sets for different sites. WP05—instrumental layout for array measurements. SESAME-Project EVG1-CT-2000-00026. Deliverable D06.05. Available via http://sesame-fp5.obs.ujf-grenoble.fr/Deliverables/D06-05_Texte.pdf. Accessed 8 May 2009

SESAME (2002b) Final report of the instrument workshop 22–26 October 2001 University of Bergen Norway. WP02—controlled instrumental specifications. SESAME-Project EVG1-CT-2000-00026. Deliverable D01.02. Available via http://sesame-fp5.obs.ujf-grenoble.fr/Deliverables/D01-02_Texte.pdf. Accessed 8 May 2009

SESAME (2005) Report on FK/SPAC capabilities and limitations. WP06—derivation of dispersion curves. SESAME-Project EVG1-CT-2000-00026. Deliverable D19.06. Available via http://sesame-fp5.obs.ujf-grenoble.fr/Deliverables/Del-D19-Wp06.pdf. Accessed 8 May 2009

Stehly L, Campillo M, Shapiro NM (2006) A study of the seismic noise from its long-range correlation properties. J Geophys Res 111:B10306. doi:10.1029/2005JB004237

Tada T, Cho I, Shinozaki Y (2006) A two-radius circular array method: inferring phase velocities of Love waves using microtremor records. Geophys Res Lett 33:L10303. doi:10.1029/2006GL025722

Tada T, Cho I, Shinozaki Y (2007) Beyond the SPAC method: exploiting the wealth of circular-array methods for microtremor exploration. Bull Seism Soc Am 97(6):2080–2095. doi:10.1785/0120070058

Tanimoto T, Alvizuri C (2006) Inversion of the HZ ratio of microseisms for S-wave velocity in the crust. Geophys J Int 165:323–335. doi:10.1111/j.1365-246.X.2006.02905.x

Tanimoto T, Ishimaru S, Alvizuri C (2006) Seasonality in particle motions of microseisms. Geophys J Int 166:253–266. doi:10.1111/j.1365-246.X.2006.02931.x

Tiberi C, Lyon-Caen H, Hatzfeld D, Achauer U, Karagianni E, Kiratzi A, LouvariE. Panagiotopoulos D, Kassaras I, Kaviris G, Makropoulos K, Papadimitriou P (2000) Crustal and upper mantle structure beneath the Corinth rift (Greece) from a teleseismic tomography study. J Geophys Res 105(B12):28159–28171

Triantafyllidis P, Hatzidimitriou PM, Suhadolc P (2001) 1-D theoretical modeling for site effect estimations in Thessaloniki: comparison with observations. Pure Appl Geophys 158:2333–2347

Triantafyllidis P, Theodulidis N, Savvaidis A, Papaioannou C, Dimitriu P (2006) Site effects estimation using earthquake and ambient noise data: the case of Lefkas town (W. Greece). 1st ECEES. Geneva, Switzerland. 3–8 September 2006, p 19

Vassalo M, Bobbio A, Iannaccone G (2008) A comparison of sea-floor and on-land seismic ambient noise in the Campi Flegrei Caldera Southern Italy. Bull Seism Soc Am 98(6):2962–2974. doi:10.1785/0120070152

Wang B, Zhu P, Chen Y, Niu F, Wang B (2008) Continuous subsurface velocity measurements with coda wave interferometry. J Geophys Res 113:B12313. doi:10.1029/2007JB005023

Wathelet M, Jongmans D, Ohrnberger M (2004) Surface-wave inversion using a direct search algorithm and its application to ambient vibration measurements. Near Surf Geophys 2:211–221

Wathelet M, Jongmans D, Ohrnberger M (2005) Direct inversion of spatial autocorrelation curves with the neighbourhood algorithm. Bull Seism Soc Am 95(5):1787–1800. doi:10.1785/0120040220

Wathelet M, Jongmans D, Ohrnberger M, Bonnefoy-Claudet S (2008) Array performance for ambient vibrations on a shallow structure and consequences over v_s inversion. J Seism 12:1–19. doi:10.1007/s10950-007-9067-x

Wegler U, Lühr B-G, Snieder R, Ratdomopurbo A (2006) Increase of shear wave velocity before the 1998 eruption of Merapi volcano (Indonesia). Geophys Res Lett 33:L09303. doi:10.1029/2006GL025928

Wilcock WSD, Webb SC, Bjarnason IT (1999) The effect of local wind on seismic noise near 1 Hz at the MELT site and in Iceland. Bull Seism Soc Am 89(6):1543–1557

Withers MM, Aster RC, Young CJ, Chael EP (1996) High-frequency analysis of seismic background noise as a function of wind speed and shallow depth. Bull Seism Soc Am 86(5):1507–1515

Yamanaka H, Dravinski M, Kagami H (1993) Continuous measurements of microtremors on sediments and basement in Los Angeles California. Bull Seism Soc Am 83(5):1595–1609

Yang J, Sato T (2000) Interpretation of seismic vertical amplification observed at an array site. Bull Seism Soc Am 90(2):275–285